



*Supplement of*

## **Comparing airborne algorithms for greenhouse gas flux measurements over the Alberta oil sands**

**Broghan M. Erland et al.**

*Correspondence to:* Broghan M. Erland (erland@ualberta.ca)

The copyright of individual parts of the supplement might differ from the article licence.

## 1 Mass-balance Box-flight Algorithm Theory Overview

The two mass-balance box-flight algorithms fundamentally differ in their parameterization of the emission flux and the mass-balance system of equations: SciAv simplifies the process to one flux and one mass-balance equation, whereas TERRA includes several flux terms to solve two mass-balance equations. Both algorithms require the same fundamental assumptions, but their approaches to quantifying the uncertainty in meeting those assumptions and estimating emissions differ. TERRA evaluates the entire dynamic system and estimates integral terms of a mass-balance equation used to derive an overall total flux (Gordon et al. 2015).

### 1.1 Top-Down Emission Rate Retrieval Algorithm (TERRA)

A strength of the TERRA model is its ability to capture and account for all the flux dynamics such as the emission vertical flux transport, chemistry, and deposition. It evaluates individual integral terms for the system of fluxes then adds them collectively. TERRA parameterizes a system of equations to derive flux and solves two mass-balance equations to estimate emissions (Gordon et al. 2015). Two common flux motions include advective transport following flow, and turbulent quasi-random, swirling traverses (Vinuesa and Galmarini 2009). The first mass balance equation for TERRA constrains the emission mixing ratio concentrations within the sampling box (the control volume), for each integral  $E$  term:

$$E_C = E_{C,H} + E_{C,HT} + E_{C,V} + E_{C,VT} + E_{C,VD} - E_{C,m} - E_{C,X} \quad (1)$$

Where  $C$  is the emission of interest (in this study  $\text{CH}_4$  or  $\text{CO}_2$ ),  $H$  the horizontal advective flux through the box walls,  $HT$  the horizontal turbulent flux through the box walls,  $V$  the advective flux through the box top,  $VT$  the turbulent flux through the box top,  $VD$  the deposition of flux to the ground,  $m$  the mass increase within the box due to air density change, and  $X$  the mass increase within the box due to chemical changes. Figure S 1 depicts the flux directions of each  $E$  integral term in Equation 1 given a cylindrical flight path to create the ‘box’. The walls of the box are the boundaries of the flight laps and arrows depict the flux that is occurring given a western wind (from the left).

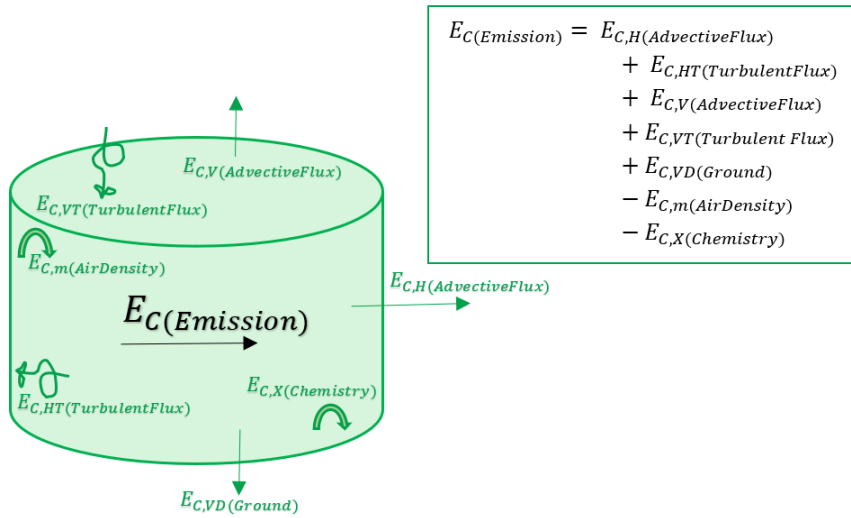


**Figure S 1: The TERRA integral E terms of Equation 1 with arrows depicting their contribution to estimating emission flux through the ‘box’, or volume.**

25 The second mass balance TERRA equation accounts for air flow in the control volume:

$$0 = E_{\text{air},H} + E_{\text{air},V} - E_{\text{air},M} \quad (2)$$

Where the three terms are:  $H$  the horizontal advective flux of air through the sides of the box,  $V$  the advective flux through the box top, and  $M$  the change in the air mass within the box respectively. The integrals are estimated using input variables derived directly from the raw data collected, or through functional equations as described in the methodology paper published by

30 Gordon et al. (2015).

There are seven error terms ( $\delta$ ) defined in methodology of TERRA that relate to the calculation of the integral terms in Equation 1 which are added in quadrature to estimate the total uncertainty ( $\delta_{\text{TERRA}}^2$ ) in the emission rate estimate (Gordon et al. 2015).

$$\delta_{\text{TERRA}}^2 = \delta_M^2 + \delta_{\text{Ex}}^2 + \delta_{\text{Wind}}^2 + \delta_{\text{Top}}^2 + \delta_{\text{dens}}^2 + \delta_{\text{VT}}^2 + \delta_{\text{BH}}^2 \quad (3)$$

35 The seven error terms in Equation 3 pertain to the uncertainty in: measurement ( $\delta_M^2$ ), near surface extrapolation of the mixing ratio ( $\delta_{\text{Ex}}^2$ ), near surface extrapolation of the wind ( $\delta_{\text{Wind}}^2$ ), the box-top mixing ratio ( $\delta_{\text{Top}}^2$ ), the change in air density ( $\delta_{\text{dens}}^2$ ), the vertical turbulent flux ( $\delta_{\text{VT}}^2$ ), and the boundary layer height ( $\delta_{\text{BH}}^2$ ). The largest error term of the method is the extrapolation of the mixing ratio from the lowest flight to the near-surface (Gordon et al. 2015). Mixing ratio surface extrapolation is chosen as either background, constant, background to constant, linear, or as an exponential fit depending on the location and dispersion  
40 of the plume and boundary layer conditions (Gordon et al. 2015). The contribution of the error of the vertical turbulent mixing term has been found to be functionally negligible and has been dropped from the overall calculation in TERRA (Baray et al. 2018; Gordon et al. 2015). The other uncertainty terms of TERRA are calculated from measuring the wind and mixing ratios, estimating the range in the box-top mixing ratio, calculating the uncertainty due to the height flown to capture the plume, and assessing atmospheric stability from the temperature and pressure ratios (Gordon et al. 2015).

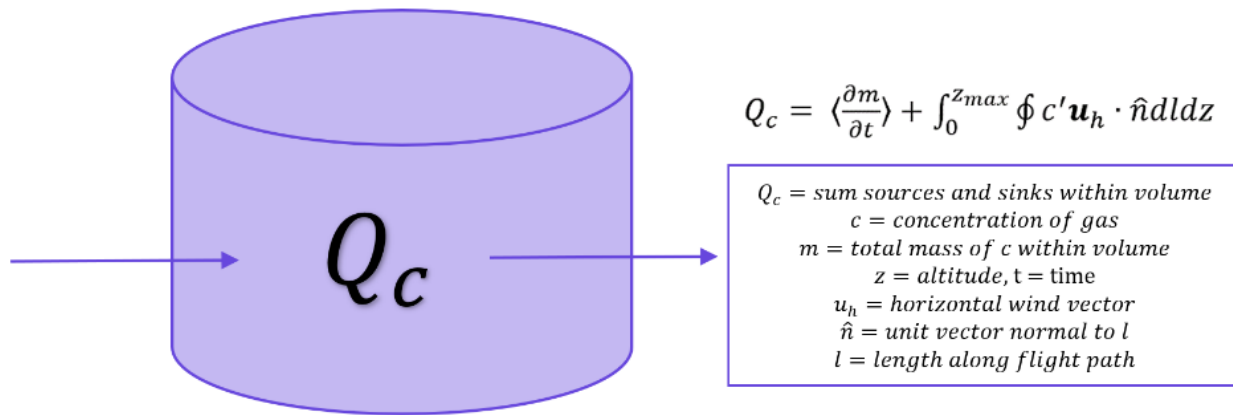
## 45 1.2 SciAv Gaussian Plume Inversion Algorithm

The SciAv model simplifies the dynamics within the box to estimate flux due to emissions from within the box. It assumes that the vertical flux is zero and that there is no flux deposition to the ground, so that only the horizontal flux needs to be estimated. As the name would suggest the Gaussian theorem algorithm utilizes Gauss's theorem, also known as the Divergence Theorem, for relating a volume integral to an integral of a surface (the laps) enclosing the volume (the box). Conley et al.

50 (2017) use the measurements to directly evaluate the balance budget of Equation 4 as described in their methods:

$$Q_c = \left\langle \frac{\partial m}{\partial t} \right\rangle + \int_0^{z_{\max}} \oint c' u_h \cdot \hat{n} dl dz \quad (4)$$

The definition of terms and diagram of the SciAv method given a cylindrical 'box', derived from the laps of the flight path, is shown in Figure S 2. Equation 4 is used to calculate the mean flux divergence for each lap. An enhancement of the mixing ratio occurs when the emission plume is captured within a lap and a positive divergence is calculated. Bins are created for ranges of altitudes and the lap estimates are aggregated into bins according to altitude and average flux values are estimated for each bin as described by Conley et al 2017. The bin averages are multiplied by the height of their respective bin then summed together. The lowest bin average is extrapolated to the ground as a constant to estimate the emission to the surface, multiplied by its bin height, then added to the other bin estimates to produce the total emission. The final flight emission estimate is the result of this discrete integration of bins of averaged lap estimates over the entire flight altitude.



60

**Figure S 2: The SciAv method simplifies the mass-balance equation to one instantaneous flux to calculate the overall horizontal sum of the source and sinks within the 'box', or volume.**

SciAv defines three error terms that are added in quadrature to estimate the uncertainty ( $\delta_{\text{SciAv}}^2$ ) in the final emission estimate:

$$\delta_{\text{SciAv}}^2 = \delta_M^2 + \delta_{\text{flux divergence}}^2 + \delta_{\text{temporal}}^2 \quad (5)$$

65

The first term is the measurement error ( $\delta_M^2$ ) which contributes the smallest amount to the final estimate error (Conley et al. 2017). The second is the flux divergence error ( $\delta_{\text{flux divergence}}^2$ ) and is calculated by summing the variance of the flux divergence estimates within each bin. The error of the surface extrapolation is estimated as twice the error of the lowest bin

and included in the flux divergence term (Conley et al. 2017). The flux divergence error accounts for the stochastic variation in plume capture for each lap and is often the largest component of the total error. The third error term is the temporal variance ( $\delta_{\text{temporal}}^2$ ) and is a measurement of the stationarity of the plume. The error due to the time rate of change is extracted from a regression of the emission density over altitude and time (Conley et al. 2017).

### Use of the TERRA Algorithm in Further Detail

To use TERRA (top-down emission rate retrieval algorithm), the appropriate surface extrapolation needed to be chosen and the emission screens assessed, the error terms calculated, and a background value calculated to use specific fits for each flight. This section outlines the processes to evaluate those four requirements as instructed by Environment and Climate Change Canada (ECCC).

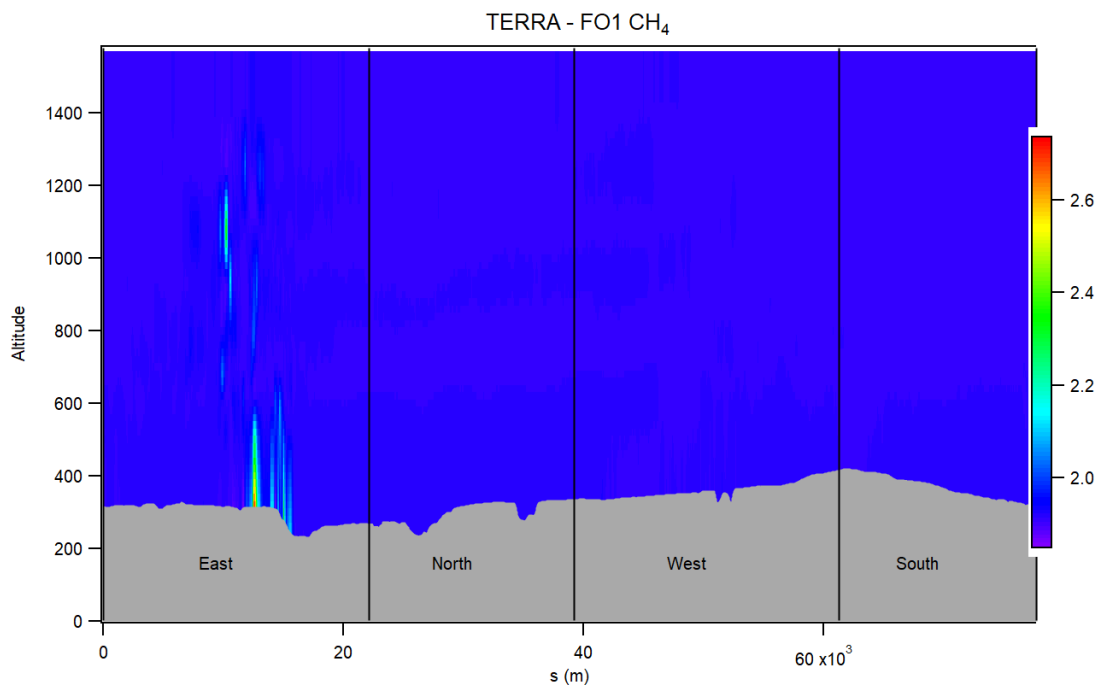
#### 1.3 TERRA Flight Screens

The emission screens produced by TERRA after fitting the chosen surface extrapolation are shown in Figure S 3 - 12. The left y-axis gives the altitude above ground level in meters, the right hand the colour scale of CH<sub>4</sub>, or CO<sub>2</sub> in ppm. The length along each lap, denoted as s(m), is plotted for each s location in meters along the x-axis with the direction of sampling overlaid. The surface is shown as grey and the gap between sampling has been filled in by the surface extrapolation. Most figures show a concentrated plume surrounded by a blue of background mixing ratio concentrations. The extent of the dispersion of the F04 CH<sub>4</sub> is noticeable in Figure S 9. The surface extrapolation sometimes estimates a decreasing emission plume towards the surface as per Figure S 4 and S 12. This leads to a larger range in the mixing ratio and a change from the typical royal blue background colour to a lighter shade such as cyan, or even light green to adjust for the lower scale. The background values are not affected by the change in colour. Aside from F04, the flight data used in the comparison analysis represent standard emissions screens for the TERRA method.

To use the interpolate, or background fit options, TERRA requires estimates of background concentrations of the desired gas present in the atmosphere, unrelated to the emission source. As part of ECCC's methodology for TERRA, ideally independent samples are gathered to estimate the background mixing ratio value of each gas for a box-flight. Background values are used in the surface extrapolation for the "background" and "linear interpolate to background" fits. The data gathered by Scientific Aviation for this analysis did not have independent samples, so the background mixing ratios were determined by inspecting the histogram of concentrations, removing the tail of enhanced emissions, then fitting a normal distribution to the values and estimating the background value as the mean of the distribution. Results are given in Table S 1. The background values used are given in Table S 2.

**Table S 1: TERRA emission rate estimates using the method’s five surface extrapolation fits in kilograms per hour for CH<sub>4</sub> and tons per hour for CO<sub>2</sub>.**

| Flight | Surface Extrapolation | CH <sub>4</sub> Emission<br>(kg h <sup>-1</sup> ) | CO <sub>2</sub> Emission<br>(t h <sup>-1</sup> ) |
|--------|-----------------------|---|--|
| F01    | Constant              | 4320  | 1220   |
| F01    | Linear                | 4810  | 1340   |
| F01    | Interpolate           | 3710  | 1040   |
| F01    | Background            | 2910  | 503  |
| F01    | Exponential           | 4460  | 1200   |
| F02    | Constant              | 412   | 535  |
| F02    | Linear                | 424   | 544  |
| F02    | Interpolate           | 395   | 515  |
| F02    | Background            | 369   | 485  |
| F02    | Exponential           | 414   | 543  |
| F03    | Constant              | 457   | 459  |
| F03    | Linear                | 476   | 467  |
| F03    | Interpolate           | 416   | 401  |
| F03    | Background            | 364   | 326  |
| F03    | Exponential           | 475   | 468  |
| F04    | Constant              | 125   | 589  |
| F04    | Linear                | 104   | 572  |
| F04    | Interpolate           | 123   | 569  |
| F04    | Background            | 119   | 543  |
| F04    | Exponential           | 122   | 589  |
| F05    | Constant              | 3540  | 882  |
| F05    | Linear                | 3910  | 877  |
| F05    | Interpolate           | 3150  | 8410   |
| F05    | Background            | 2630  | 790  |
| F05    | Exponential           | 3680  | 1220   |



105 **Figure S 3: The TERRA screen for F01 CH<sub>4</sub> in ppm. Altitude measured in meters is shown along the left y-axis and the colour bar on the right depicts the mixing ratio gradient in ppm. The s location along each lap in meters, all in scientific notation, is plotted along the x-axis as s(m) with the direction of sampling overlaid. The ground is shown in grey.**

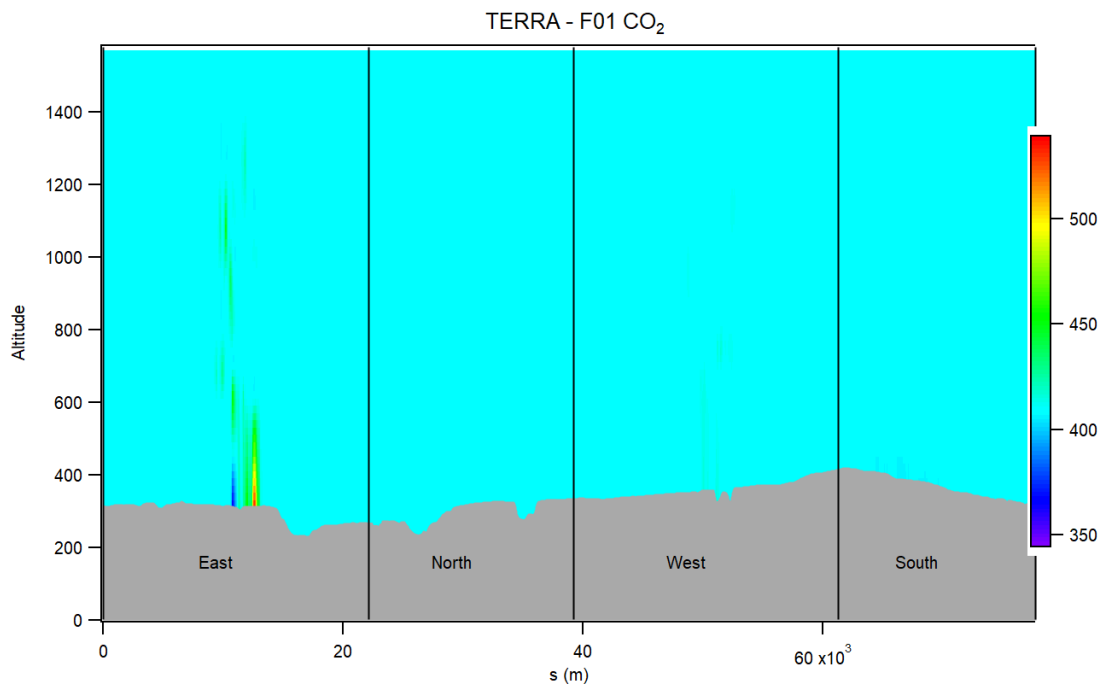
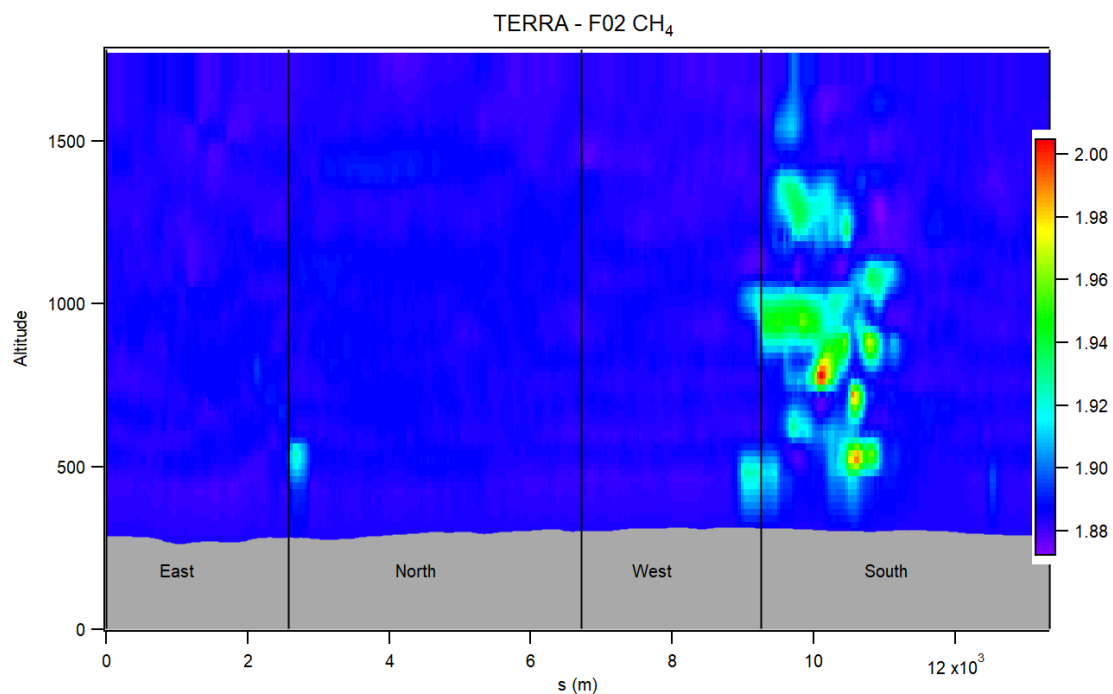


**Figure S 4: Same as Figure S 3 for flight F01 CO<sub>2</sub> (ppm).**



110 **Figure S 5: Same as Figure S 3 for flight F02 CH<sub>4</sub> (ppm).**

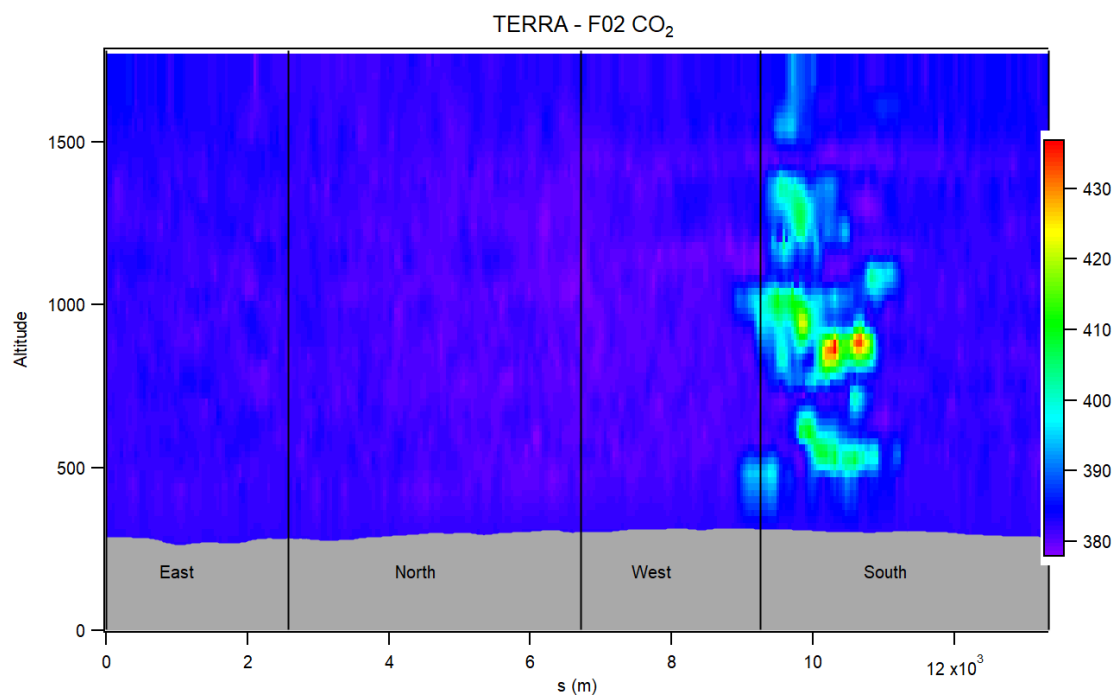


**Figure S 6: Same as Figure S 3 for flight F02 CO<sub>2</sub> (ppm).**



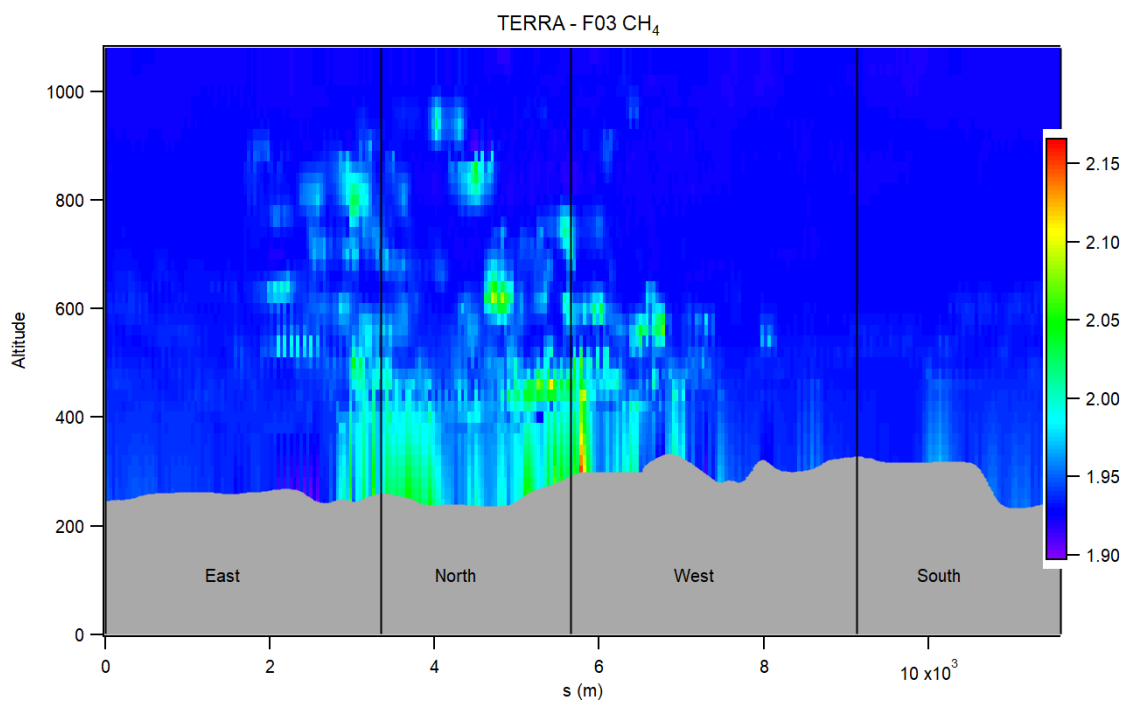


**Figure S7: Same as Figure S 3 for flight F03 CH<sub>4</sub> (ppm).**

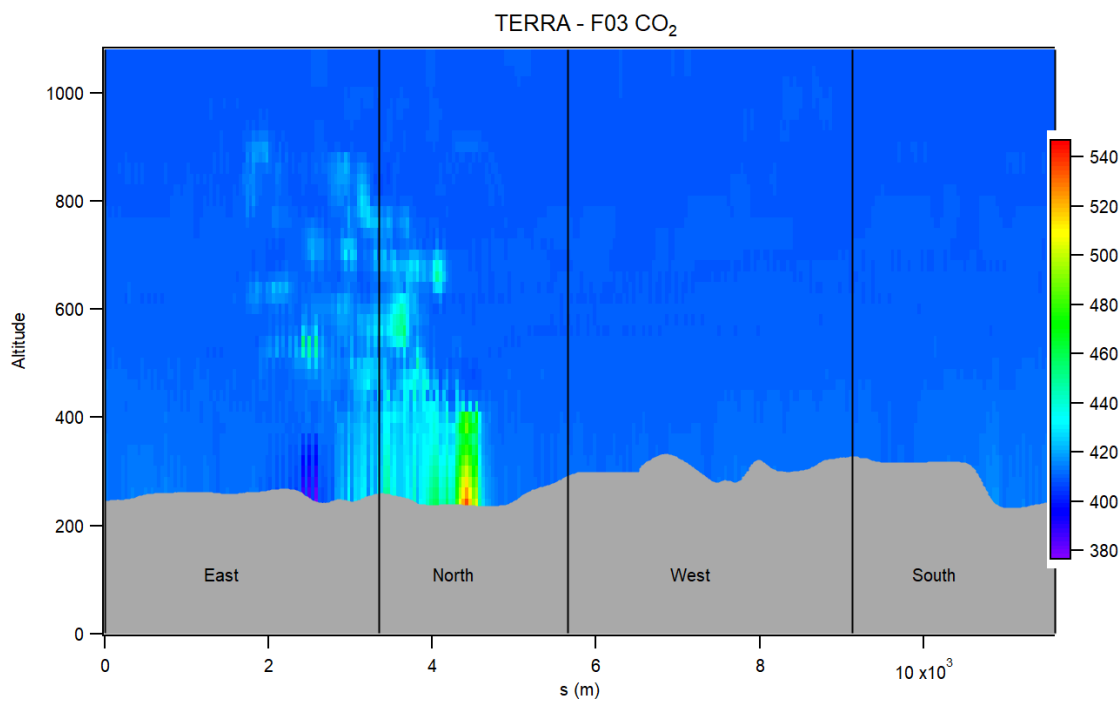


**Figure S 8: Same as Figure S 3 for flight F03 CO<sub>2</sub> (ppm).**

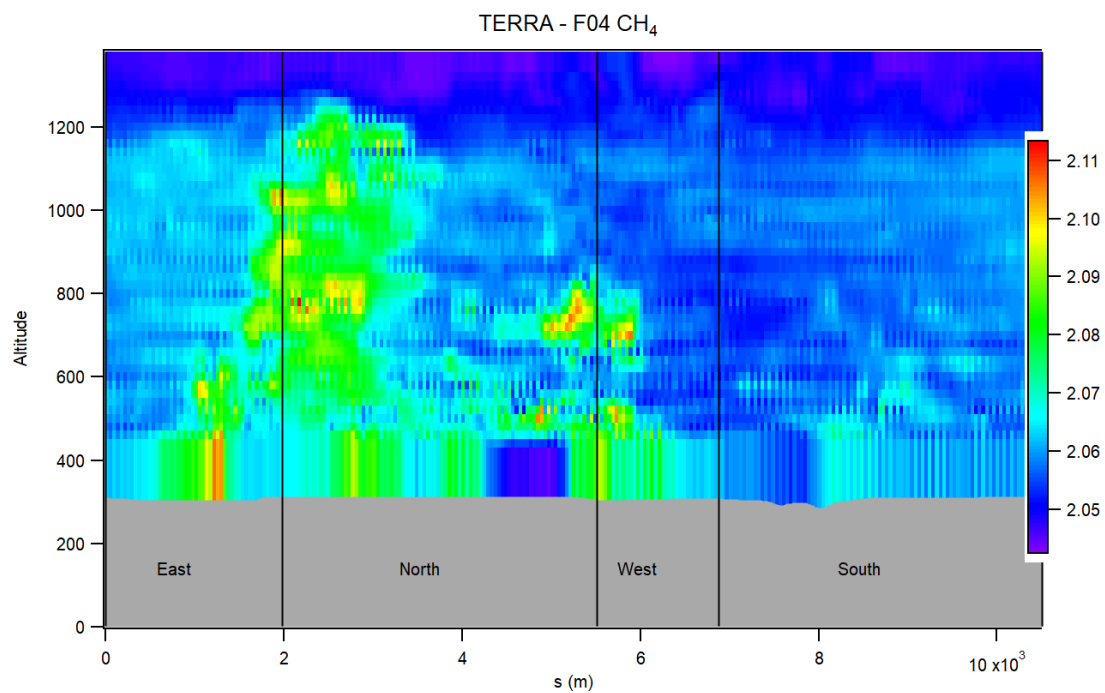
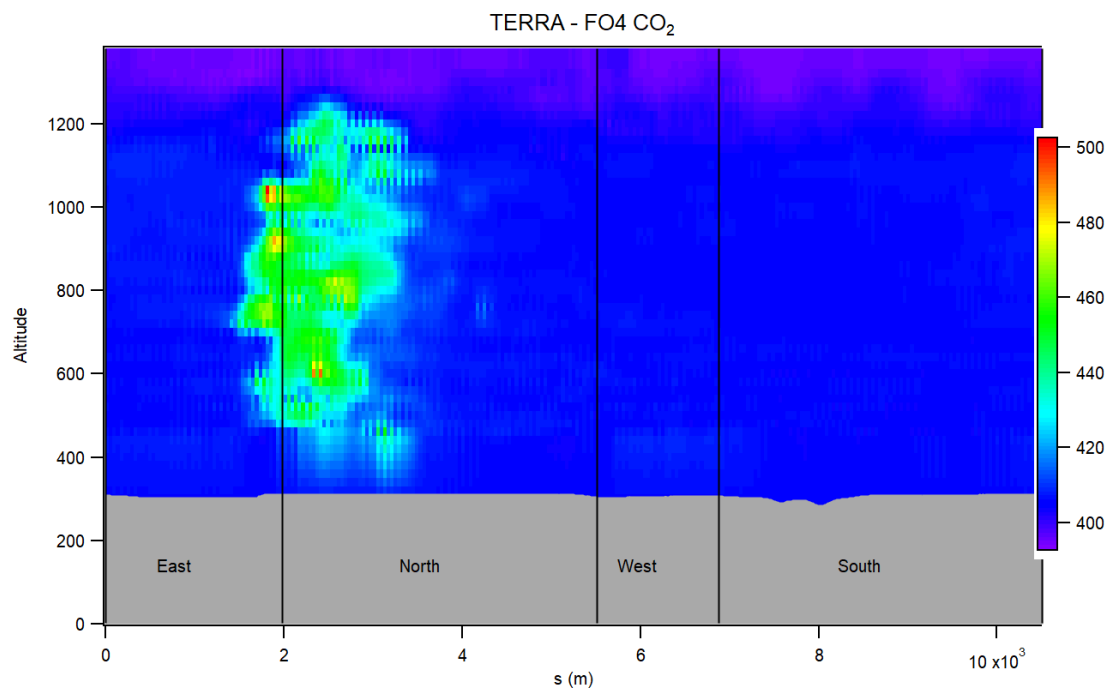


**Figure S 9: Same as Figure S 3 for flight F04 CH<sub>4</sub> (ppm).**



**120 Figure S 10: Same as Figure S 3 for flight F04 CO<sub>2</sub> (ppm).**

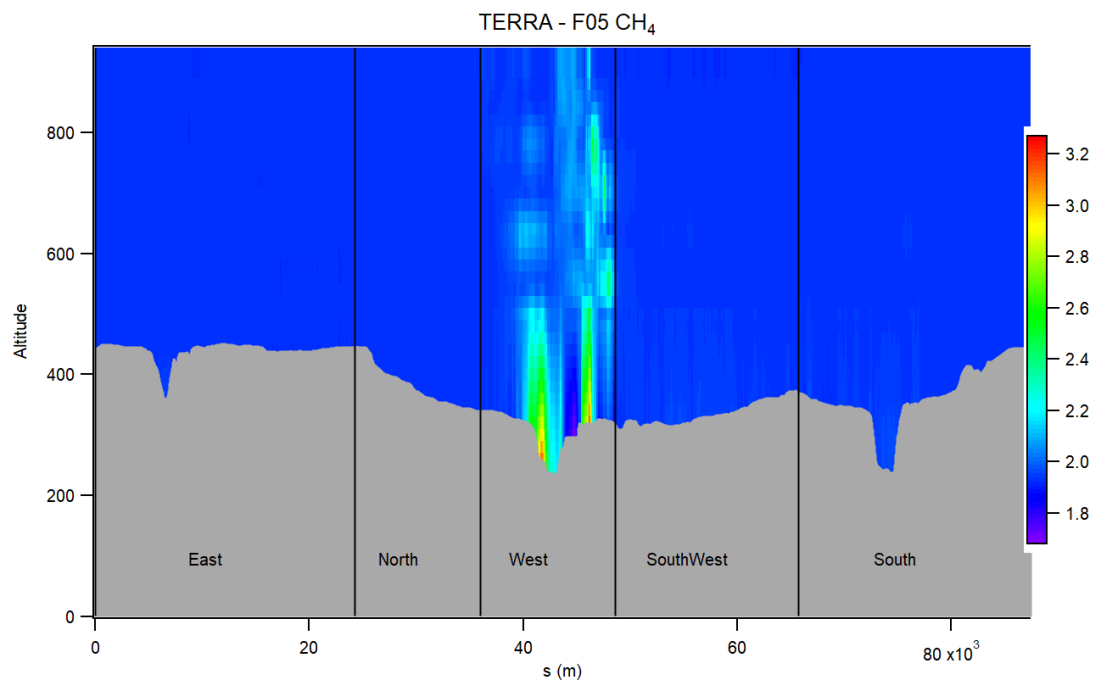


**Figure S 11: Same as Figure S 3 for flight F05 CH<sub>4</sub> (ppm).**

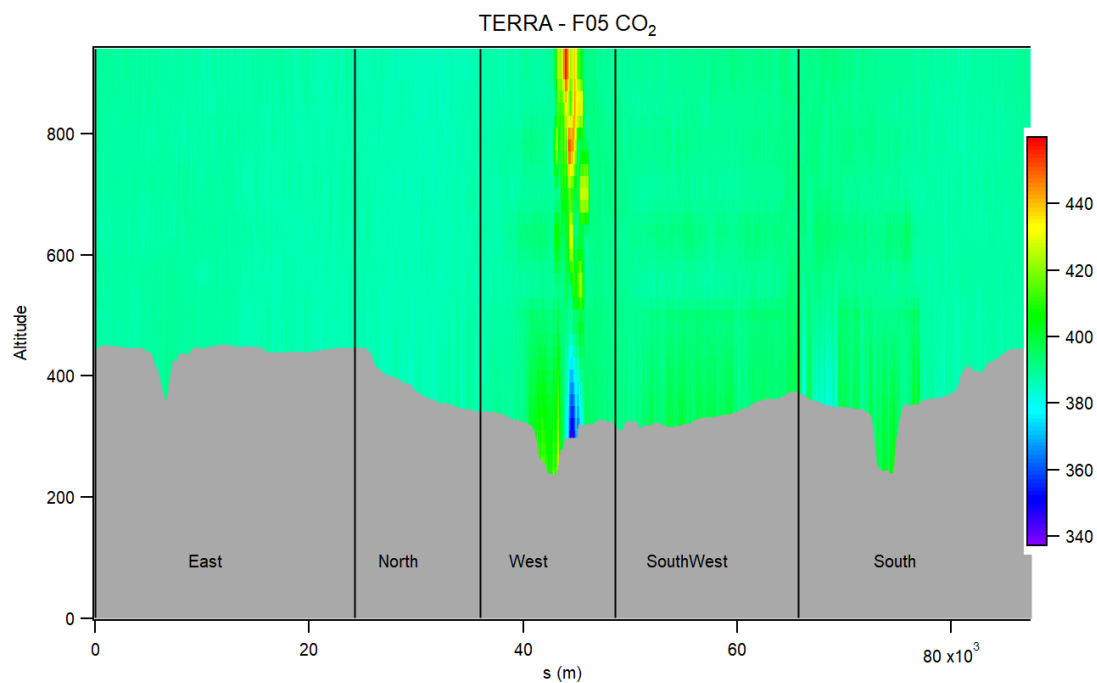


**Figure S 12: Same as Figure S 3 for flight F05 CO<sub>2</sub> (ppm).**

**Table S 2: Background mixing ratio values used in the surface extrapolation of each flight.**

| Flight | CH <sub>4</sub> (ppm) | CO <sub>2</sub> (ppm) |
|--------|-----------------------|-----------------------|
| F01    | 1.91613               | 409.1896              |
| F02    | 1.88481               | 382.3219              |
| F03    | 1.93007               | 410.2672              |
| F04    | 2.05365               | 405.8721              |
| F05    | 1.93103               | 389.4703              |

**1.4 TERRA Error Terms**

The calculated TERRA error terms are provided in Table S 3 and descriptions of how the terms were calculated are detailed in this section.

130

The box-top mixing ratio error is assumed to be normally distributed and is calculated as the percent change in the 95% confidence interval of the mean mixing ratio at the box top. The confidence interval was computed as the mean value  $\pm 2\sigma/\sqrt{n}$ , where  $\sigma$  is the standard deviation of measurements and  $n$  the number of independent samples (Gordon et al., 2015). The value of  $n$  is determined by the length of a single lap divided by the length scale which was conservatively set to 3km as a maximum of the distance needed for the autocorrelation of the mixing ratio series to approach zero (Gordon et al., 2015).

135

To calculate the density, change error air pressure and temperature measurements were extracted from independent towers near the sampling area. Four towers were identified near the flight locations: two at the Fort McMurray Airport (A and CS at 56.65 °N, 111.22° W, <http://climate.weather.gc.ca>) and the Wood Buffalo Environmental Association’s JP104 (57.12 °N, 111.43° W) and JP311 (56.56°N, 111.95° W) meteorological towers (<http://wbea.org>). Average, maximum, and minimum changes in the ratio difference of pressure and temperature ( $\Delta p_i/p_i - \Delta T_i/T_i$ ) among the four stations were calculated then used to estimate total emissions using those values (Gordon et al., 2015). The uncertainty percentage was then calculated as the uncertainty range between  $E_{max}/E$  to  $E_{min}/E$ .

140

The box top height error was calculated in IGOR 8 using TERRA by estimating the percent change in the final emission estimate when the screen produced from kriging is redrawn 100 m lower. ECCC was only able to provide two flights with a redrawn box for analysis, therefore two examples of the average, and extreme case for plume capture were used. Redrawn screens were provided by ECCC for two of the flights representing the change given a ‘fully captured’ plume (F01), and a sample when the plume still had large enhancements at the top of the flight (F05). As part of a preliminary analysis of flights

145

150 from the larger Alberta Campaign, AEP and Scientific Aviation deemed F02, F03, and F04 to have ‘fully captured’ the top of the emission plume. Therefore, the F01 error was rounded up to the nearest integer and used to estimate the box top height errors for F02, F03, and F04.

155 **Table S 3: TERRA emission estimate uncertainties as a percentage of the total emission estimate. Error terms are added in quadrature to give the total percentage uncertainty ( $\delta$ ). Wind and measurement error were added in quadrature as values of 1 and the vertical turbulence term was dropped from the calculation.**

| Flight                | Measurement Error $\delta_M$ | Mixing ratio Extrapolation $\delta_{Ex}$ | Wind Extrapolation $\delta_{Wind}$ | Box-top mixing ratio $\delta_{Top}$ | Density Change $\delta_{dens}$ | Vertical Turbulence $\delta_{VT}$ | Box-top height $\delta_{BH}$ | Total Uncertainty $\delta$ |
|-----------------------|------------------------------|--|------------------------------------|-------------------------------------|--------------------------------|-----------------------------------|------------------------------|----------------------------|
| F01 - CH <sub>4</sub> | <1%                          | 10.13                                    | <1%                                | 0.89                                | 0.03                           | N/A                               | 0.56                         | 10.28                      |
| F01 - CO <sub>2</sub> | <1%                          | 10.04                                    | <1%                                | 0.89                                | 0.02                           | N/A                               | 0.35                         | 10.18                      |
| F02 - CH <sub>4</sub> | <1%                          | 4.80                                     | <1%                                | 2.15                                | 1.06                           | N/A                               | 1                            | 5.64                       |
| F02 - CO <sub>2</sub> | <1%                          | 5.43                                     | <1%                                | 0.38                                | 0.89                           | N/A                               | 1                            | 5.78                       |
| F03 - CH <sub>4</sub> | <1%                          | 4.16                                     | <1%                                | 2.30                                | 0.48                           | N/A                               | 1                            | 5.08                       |
| F03 - CO <sub>2</sub> | <1%                          | 1.71                                     | <1%                                | 2.30                                | 0.83                           | N/A                               | 1                            | 3.45                       |
| F04 - CH <sub>4</sub> | <1%                          | 17.08                                    | <1%                                | 2.42                                | 5.79                           | N/A                               | 1                            | 18.28                      |
| F04 - CO <sub>2</sub> | <1%                          | 3.53                                     | <1%                                | 2.43                                | 4.93                           | N/A                               | 1                            | 6.76                       |
| F05 - CH <sub>4</sub> | <1%                          | 9.54                                     | <1%                                | 1.00                                | 0.04                           | N/A                               | 11.17                        | 14.79                      |
| F05 - CO <sub>2</sub> | <1%                          | 7.33                                     | <1%                                | 1.11                                | 0.10                           | N/A                               | 24.82                        | 25.94                      |

**Adaptation of the SciAv Method in Further Detail**

The raw data files for the five flights can be accessed through the Government of Alberta Portal:

160 <http://ckandata01.canadacentral.cloudapp.azure.com/dataset/aep-noaa-greenhouse-gas-measurement-flights>

The calculated average divergence for each lap, and associated errors provided by Scientific Aviation are provided in Table S 4. The lap bin bounds also provided by Scientific Aviation are given in Table S 5. Together these data can be used to recreate the SciAv profiles and emission calculations for each flight.

**Table S 4: The average flux divergence and uncertainty for each flight lap.**

| Flight | Lap Number | Altitude (m) | CH <sub>4</sub> Average Flux Divergence | CH <sub>4</sub> Uncertainty | CO <sub>2</sub> Average Flux Divergence | CO <sub>2</sub> Uncertainty |
|--------|------------|--------------|---|-----------------------------|---|-----------------------------|
| F01    | 1          | 168.3        | 10.1355                                 | 1.2505                      | 3088.564                                | 572.941                     |
|        | 2          | 319.1        | 3.0669                                  | 0.4684                      | 1596.195                                | 359.556                     |
|        | 3          | 614.8        | 3.2761                                  | 0.5843                      | 722.717                                 | 185.185                     |
|        | 4          | 912.6        | 2.5053                                  | 0.3873                      | 470.83                                  | 104                         |
|        | 5          | 1056.9       | 0.2748                                  | 0.0572                      | -65.667                                 | 26.51                       |
|        | 6          | 771.2        | 4.0707                                  | 1.0834                      | 862.677                                 | 280.279                     |
|        | 7          | 464.3        | 3.1503                                  | 0.3544                      | 706.667                                 | 97.554                      |
|        | 8          | 378.6        | 2.5528                                  | 0.3681                      | 614.653                                 | 182.681                     |
| F02    | 1          | 173          | 0.2896                                  | 0.0831                      | 392.011                                 | 81.71                       |
|        | 2          | 301.6        | 0.2762                                  | 0.0713                      | 428.288                                 | 107.227                     |
|        | 3          | 454.7        | 0.3529                                  | 0.1409                      | 439.68                                  | 76.177                      |
|        | 4          | 614.6        | 0.7203                                  | 0.1425                      | 805.679                                 | 149.198                     |
|        | 5          | 778.3        | 0.1679                                  | 0.0682                      | 379.872                                 | 81.875                      |
|        | 6          | 919.3        | 0.1575                                  | 0.0689                      | 286.82                                  | 81.201                      |
|        | 7          | 1076.7       | 0.1021                                  | 0.0688                      | 227.823                                 | 82.947                      |
|        | 8          | 1245.6       | 0.0194                                  | 0.0327                      | 120.558                                 | 44.357                      |
|        | 9          | 1122.5       | -0.0992                                 | 0.0231                      | -26.271                                 | 24.561                      |
|        | 10         | 863.2        | -0.013                                  | 0.0299                      | 224.649                                 | 84.076                      |
|        | 11         | 714.1        | 0.5437                                  | 0.0871                      | 786.83                                  | 129.209                     |
|        | 12         | 546.2        | 0.7292                                  | 0.1357                      | 1355.712                                | 261.852                     |
|        | 13         | 407.8        | 0.2934                                  | 0.0943                      | 169.528                                 | 60.786                      |
|        | 14         | 247.7        | 0.4213                                  | 0.1408                      | 726.796                                 | 146.438                     |
| F03    | 1          | 217          | 0.64                                    | 0.264                       | 0.981                                   | 0.16                        |
|        | 2          | 190          | 0.896                                   | 0.142                       | 1.358                                   | 0.293                       |
|        | 3          | 146          | 0.713                                   | 0.151                       | 1.065                                   | 0.17                        |
|        | 4          | 163          | 0.572                                   | 0.218                       | 0.513                                   | 0.088                       |
|        | 5          | 189          | 0.71                                    | 0.329                       | 0.732                                   | 0.117                       |
|        | 6          | 238          | 0.651                                   | 0.166                       | 0.708                                   | 0.121                       |
|        | 7          | 273          | 0.635                                   | 0.132                       | 0.687                                   | 0.141                       |
|        | 8          | 305          | 0.232                                   | 0.159                       | 0.698                                   | 0.105                       |
|        | 9          | 351          | 0.952                                   | 0.14                        | 0.729                                   | 0.1                         |
|        | 10         | 411          | 1.216                                   | 0.133                       | 1.404                                   | 0.165                       |
|        | 11         | 479          | 0.534                                   | 0.126                       | 0.789                                   | 0.085                       |
|        | 12         | 760          | -0.06                                   | 0.021                       | -0.034                                  | 0.007                       |
|        | 13         | 743          | -0.086                                  | 0.014                       | -0.022                                  | 0.005                       |
|        | 14         | 685          | 0.394                                   | 0.095                       | 0.089                                   | 0.006                       |
|        | 15         | 630          | 0.363                                   | 0.054                       | 0.233                                   | 0.027                       |
|        | 16         | 541          | 1.693                                   | 0.137                       | 0.366                                   | 0.052                       |
|        | 17         | 599          | 0.854                                   | 0.083                       | 0.467                                   | 0.07                        |
|        | 18         | 377          | 1.166                                   | 0.272                       | 0.439                                   | 0.064                       |
|        | 19         | 270          | -0.383                                  | 0.282                       | 1.454                                   | 0.173                       |
| F04    | 1          | 149.6        | 0.2452                                  | 0.0907                      | 410.132                                 | 101.242                     |

|     |    |        |         |        |          |          |
|-----|----|--------|---------|--------|----------|----------|
|     | 2  | 213.1  | 0.426   | 0.0818 | 542.878  | 100.554  |
|     | 3  | 271.9  | 0.533   | 0.0776 | 1481.367 | 243.59   |
|     | 4  | 334.2  | 0.2294  | 0.0768 | 705.472  | 176.109  |
|     | 5  | 404    | 0.3517  | 0.0959 | 1265.809 | 247.591  |
|     | 6  | 461.4  | 0.6256  | 0.0987 | 1888.899 | 358.211  |
|     | 7  | 524.4  | 0.6017  | 0.0773 | 2187.546 | 330.685  |
|     | 8  | 593.1  | 0.4238  | 0.0633 | 1784.319 | 299.135  |
|     | 9  | 657.3  | 0.29    | 0.0487 | 1041.434 | 164.144  |
|     | 10 | 725.1  | 0.3704  | 0.0755 | 1836.424 | 375.014  |
|     | 11 | 782.3  | 0.4037  | 0.0505 | 1402.95  | 202.694  |
|     | 12 | 847.4  | 0.3731  | 0.0652 | 1396.115 | 239.28   |
|     | 13 | 908.1  | 0.4542  | 0.0599 | 1293.877 | 176.586  |
|     | 14 | 985.6  | -0.0459 | 0.0167 | -102.74  | 37.426   |
|     | 15 | 1042.2 | -0.0654 | 0.013  | 114.457  | 15.781   |
|     | 16 | 926.7  | 0.2604  | 0.0403 | 861.268  | 146.277  |
|     | 17 | 837.5  | 0.1892  | 0.0601 | 708.29   | 207.149  |
|     | 18 | 745.7  | 0.3288  | 0.0589 | 968.067  | 194.864  |
|     | 19 | 653.6  | 0.3971  | 0.0467 | 1426.952 | 186.054  |
|     | 20 | 558.2  | 0.3413  | 0.0629 | 1543.505 | 230.08   |
|     | 21 | 468.5  | 0.3703  | 0.0649 | 1323.173 | 180.568  |
|     | 22 | 374.6  | 0.387   | 0.0648 | 1197.24  | 255.098  |
|     | 23 | 280.2  | 0.3741  | 0.0591 | 1448.465 | 316.375  |
|     | 24 | 211.6  | 0.3401  | 0.0593 | 1123.024 | 248.665  |
|     | 25 | 159    | 0.2561  | 0.0724 | 1143.119 | 212.599  |
| F05 | 1  | 157.2  | 7.8943  | 4.2509 | 1134.799 | 542.43   |
|     | 2  | 306.6  | 7.9906  | 2.7143 | 1929.259 | 686.358  |
|     | 3  | 455.8  | 8.117   | 3.0318 | 2176.205 | 1094.005 |
|     | 4  | 562.7  | 3.6854  | 1.5554 | 2296.309 | 1159.373 |
|     | 5  | 508.5  | 3.6561  | 1.4827 | 1717.746 | 1048.646 |
|     | 6  | 359.7  | 6.0673  | 2.7987 | 1119.228 | 812.077  |
|     | 7  | 211.7  | 5.0426  | 3.222  | 611.016  | 578.053  |

165

170

Table S 5: The profile altitude bin bounds provided by Scientific Aviation.

| Flight | Bin Lower Limit<br>(m) | Bin Middle<br>(m) | Bin Upper Limit<br>(m) |
|--------|------------------------|-------------------|------------------------|
| F01    | 0                      | 84.1              | 168.3                  |
|        | 168.3                  | 316.4             | 464.5                  |
|        | 464.5                  | 612.6             | 760.7                  |
|        | 760.7                  | 908.8             | 1056.9                 |
| F02    | 0                      | 86.5              | 173                    |
|        | 173                    | 307               | 441.1                  |
|        | 441.1                  | 575.2             | 709.3                  |
|        | 709.3                  | 843.3             | 977.4                  |
|        | 977.4                  | 1111.5            | 1245.6                 |
| F03    | 0                      | 69.59             | 139.18                 |
|        | 139.18                 | 202.76            | 266.34                 |
|        | 266.34                 | 329.92            | 393.5                  |
|        | 393.5                  | 457.08            | 520.66                 |
|        | 520.66                 | 584.23            | 647.81                 |
|        | 647.81                 | 711.39            | 774.97                 |
| F04    | 0                      | 74.8              | 149.6                  |
|        | 149.6                  | 238.9             | 328.1                  |
|        | 328.1                  | 417.4             | 506.6                  |
|        | 506.6                  | 595.9             | 685.2                  |
|        | 685.2                  | 774.4             | 863.7                  |
|        | 863.7                  | 952.9             | 1042.2                 |
| F05    | 0                      | 78.6              | 157.2                  |
|        | 157.2                  | 258.6             | 359.9                  |
|        | 359.9                  | 461.3             | 562.7                  |



1.5 Fitting the SciAv Surface Extrapolation

The following section provides the Scientific Aviation (SciAv) algorithm surface extrapolation for all five different fits: Constant, Linear, Interpolate, Background, and Linear Weighted. The algorithm’s integration method of binning the estimates and add adding in summation the average of each bin was applied for the measured part of the profile (Conley et al., 2017). For each surface extrapolation the lowest bin was extrapolated to the surface using the given fit. Certain profile shapes can be used to determine the fitting height depending on the number of points, minimum height, and shape of the bottom of the profile. The chosen fitting heights were: 1100m for F01, 400m for F02, 250m for F03, 400m for F04, and 600m for F05. The final estimate was determined by combining the emissions calculated from binned profile added to the trapezoidal integration of area between the extrapolation fit, the surface, and a flux enhancement of zero (main text, Figure 4). The estimates produced by fitting the different surface extrapolations to SciAv are given in Table S 6. Figure S 13A shows that both emission profiles for F01 follows a type III shape with fits for linear, weighted linear, and averaged increasing towards the surface. The F01 surface extrapolation and resulting emission estimate would be larger and more closely follow plume behaviour if the lowest divergence point, rather than the lowest bin estimate (the method standard), was used (Figure S 13 A). The F02 SciAv profile follows a Type II shape (Figure S 13 B) with very little variation in the extrapolation fits, which are clustered around the standard constant fit. The F03 SciAv profile has a lot of between-lap variation with a profile shape that largely follows a Type I shape (Figure S 13 C). The F03 surface extrapolation was the most unstable fit due to the larger variation between laps at the bottom of the profiles. F05 was the only flight with varying profile shapes for and CH<sub>4</sub> and CO<sub>2</sub>. The shape of the emission profile in Figure S 13 E for CH<sub>4</sub> shows some constraining of the plume at the highest altitude; however, the divergence is still larger than 2 kg m<sup>-1</sup> hr<sup>-1</sup> which is larger than the peak of divergence from plant samples. The profile for F05 in Figure S 13 E shows incomplete sampling for CO<sub>2</sub> as the divergence points are still increasing at the highest altitude indicating that the plume was not fully captured.

200 **Table S 6: SciAv emission rate estimates using six surface extrapolation fits.**

| Flight | Surface Extrapolation | CH <sub>4</sub> Emission (kg h <sup>-1</sup> ) | CO <sub>2</sub> Emission (t h <sup>-1</sup> ) |
|--------|-----------------------|--|---|
| F01    | Constant              | 3840   | 1040  |
| F01    | Linear                | 5270   | 1250  |
| F01    | Interpolate           | 3900   | 1040  |
| F01    | Background            | 3050   | 784   |
| F01    | Linear Weighted       | 4690   | 1300  |
| F01    | Averaged              | 4200   | 1150  |
| F02    | Constant              | 362  | 5630  |
| F02    | Linear                | 360  | 556   |
| F02    | Interpolate           | 331  | 523   |

|     |                 |      |      |
|-----|-----------------|------|------|
| F02 | Background      | 306  | 489  |
| F02 | Linear Weighted | 359  | 563  |
| F02 | Averaged        | 361  | 562  |
| F03 | Constant        | 497  | 526  |
| F03 | Linear          | 506  | 553  |
| F03 | Interpolate     | 452  | 479  |
| F03 | Background      | 400  | 401  |
| F03 | Linear Weighted | 504  | 571  |
| F03 | Averaged        | 503  | 548  |
| F04 | Constant        | 349  | 1170 |
| F04 | Linear          | 332  | 1090 |
| F04 | Interpolate     | 313  | 1050 |
| F04 | Background      | 295  | 1020 |
| F04 | Linear Weighted | 332  | 1110 |
| F04 | Averaged        | 341  | 1140 |
| F05 | Constant        | 3470 | 850  |
| F05 | Linear          | 3710 | 783  |
| F05 | Interpolate     | 3030 | 751  |
| F05 | Background      | 2410 | 661  |
| F05 | Linear Weighted | 3670 | 782  |
| F05 | Averaged        | 3590 | 1040 |

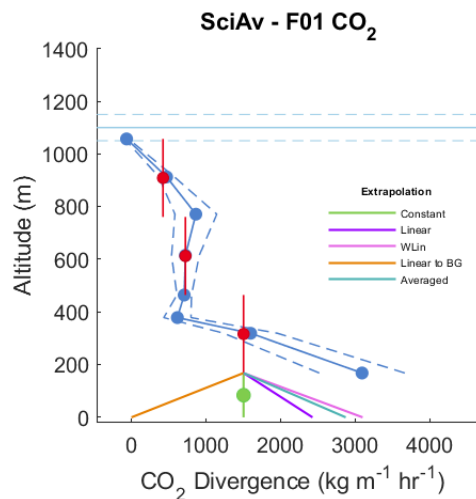
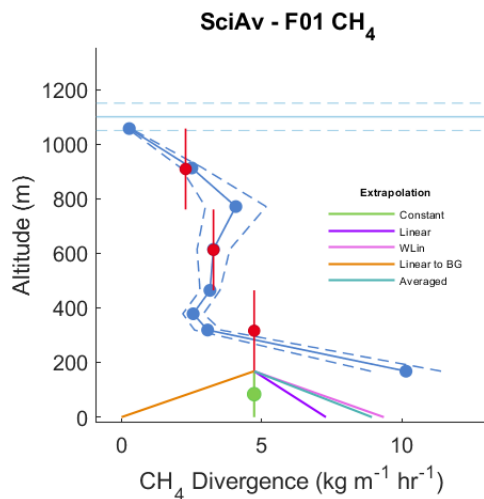


**Figure S 13 A**

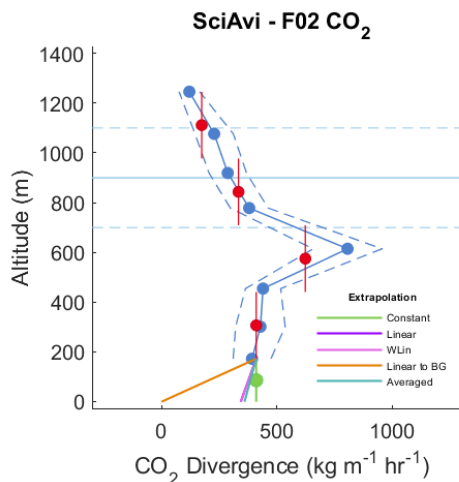
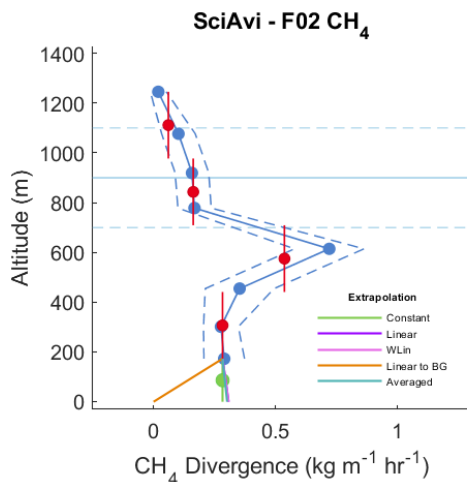


**Figure S 13 B**

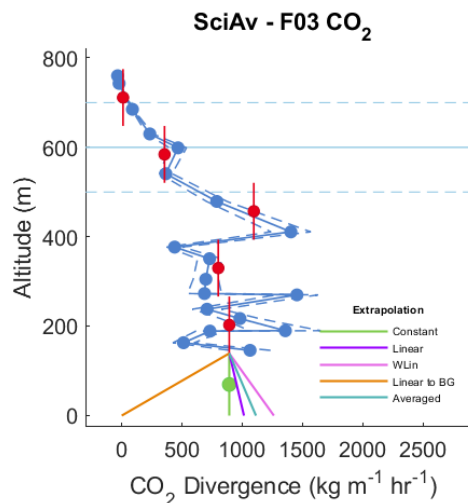
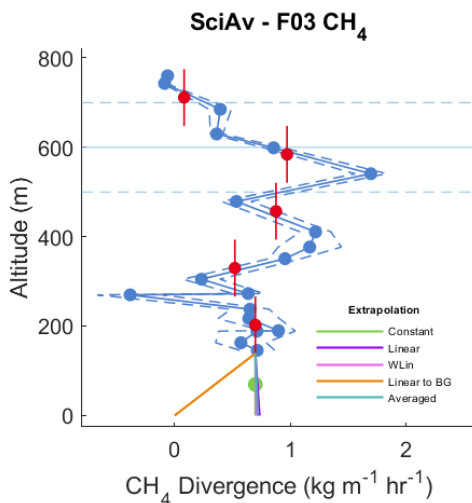


**Figure S 13 C**

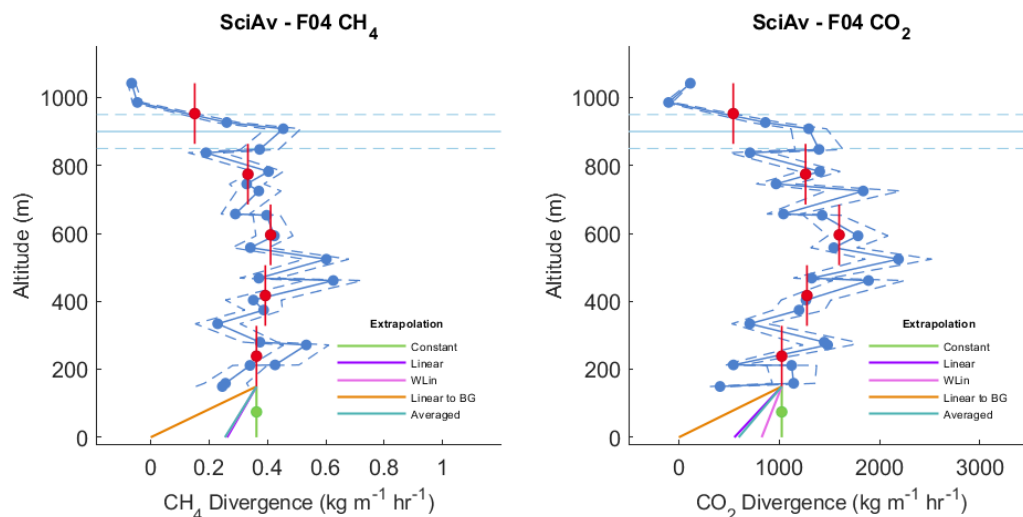


Figure S 13 D.

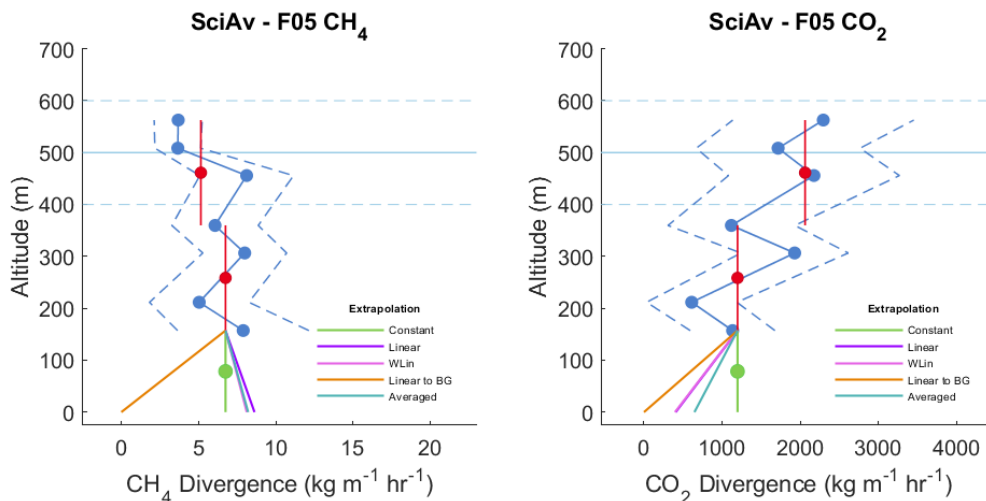


Figure S 13 E.

Figure S 13: The SciAv profile is shown for F01-F05 in Figures S 13A – 13E. The blue points are the estimated flux divergence for each lap which are connected to show profile shape with the associated error (a dashed blue line). Red points are bin averages and the vertical red bar is the bin height range. The boundary layer height is drawn in light blue with error bars (light blue dashed lines). The five surface extrapolations are drawn from the bottom of the lowest red bin.

Comparison of SciAv and TERRA Methods Extended

205 1.6 Significance Testing and Further Comparison

The difference between estimates, relative mean percentage difference, and the propagated error in percentage for the average estimate of the two algorithms are shown in Table S 7. The whole set of results from five flights were formally tested for differences between the SciAv and TERRA estimates using a weighted t-test and Wilcoxon signed rank test. As a collective, the differences between the estimates were found to be insignificant for both CH<sub>4</sub> and CO<sub>2</sub> (Table S 8).

210

**Table S 7: Differences between algorithms as SciAv estimate – TERRA estimate for each flight, relative percentage differences and the propagated percentage error of the estimates. A mean percentage difference that is approximately equal to, or smaller than the propagated percentage error of the estimates indicates agreement within the uncertainty of the estimates.**

215

|  | F01     | F02   | F03   | F04    | F05    |
|--|---------|-------|-------|--------|--------|
| CH <sub>4</sub> : Difference (kg h <sup>-1</sup> ) | -967    | -33.5 | 20.5  | 224    | -436   |
| CH <sub>4</sub> : Relative Percentage Difference   | 22%     | 8%    | 4%    | 94%    | 12%    |
| CH <sub>4</sub> : Propagated Percentage Error      | 21%     | 22%   | 17%   | 18%    | 29%    |
| CO <sub>2</sub> : Difference (kg h <sup>-1</sup> ) | -302000 | 47900 | 58700 | 602000 | -27700 |
| CO <sub>2</sub> : Relative Percentage Difference   | 25%     | 9%    | 12%   | 69%    | 3%     |
| CO <sub>2</sub> : Propagated Percentage Error      | 24%     | 19%   | 12%   | 13%    | 43%    |

220

**Table S 8: Results of parametric (weighted t-test) and non-parametric (Wilcoxon signed-rank test) significance testing of differences between the two box-flight algorithms using the set of all five flight estimates.**

|                 | Weighted t-test: p-value | Weighted t-test: t-value | Wilcoxon signed-rank test: p-value | Wilcoxon signed-rank test: V |
|-----------------|--------------------------|--------------------------|------------------------------------|------------------------------|
| CH <sub>4</sub> | 0.306                    | -1.09                    | 0.438                              | 4                            |
| CO <sub>2</sub> | 0.366                    | -0.96                    | 0.625                              | 10                           |

225

To remove the effect of the surface extrapolation the two algorithms were compared when using each method’s “background” surface extrapolation fit. For TERRA this meant fitting the chosen background mixing ratio value below the lowest flight lap, and for SciAv calculating zero divergence below the lowest flight lap. Neither algorithm would choose background extrapolation for the standard estimate to the flights as increasing or trace emissions were present at the bottom of each the flight track.

230

The results of calculations using the assumption of no emission plume below the lowest flight track were compared to the standard fit in Figure S 12. The estimate uncertainties were only calculated for each algorithm’s standard fit, therefore estimates using other fits have no error bars. The mean of the surface extrapolation estimates and the difference between the

mean estimates is given in Table S 9. Results of parametric (weighted t-test) and non-parametric (Wilcoxon signed-rank test) significance testing of differences between the two box-flight algorithms using the set of all five flights given each the standard fit, background fit, and average of the fits estimates is given in Table S 9.

235 Emission estimates using a background fit are systematically lower than the standard estimates (Figure S 14), but no clear pattern is identifiable that would indicate systematic disagreement. There is a considerably larger TERRA estimate for F01 between the standard fit compared to the background. The choice of surface extrapolation influences the extent of agreement. The algorithms tend to agree more when the effect of a different surface extrapolation is removed as much as possible. This indicates good agreement between the methods. When fundamental assumptions are met, variation between the estimates can largely be attributed to different surface extrapolation methods.

240

**Table S 9: The mean differences between the two algorithm outputs amongst the five flights and results from significance testing were calculated for comparison between the standard, background and average of the algorithms fit.**

|  | CH <sub>4</sub><br>Standard | CH <sub>4</sub><br>Background | CH <sub>4</sub><br>Average | CO <sub>2</sub><br>Standard | CO <sub>2</sub><br>Background | CO <sub>2</sub><br>Average |
|--|-----------------------------|-------------------------------|----------------------------|-----------------------------|-------------------------------|----------------------------|
| Mean Difference<br>(kg h <sup>-1</sup> ) | -239                        | 12.4                          | 47.8                       | 75800                       | 141000                        | 115000                     |
| Pairwise t-test: p-value                 | 0.857                       | 0.989                         | 0.969                      | 0.724                       | 0.321                         | 0.525                      |
| Pairwise t-test: t-value                 | -0.187                      | 0.0145                        | 0.0404                     | 0.367                       | 1.07                          | 0.665                      |
| Wilcoxon signed-rank test: p-value       | 0.438                       | 1                             | 0.625                      | 0.625                       | 0.313                         | 0.313                      |
| Wilcoxon signed-rank test: V             | 4                           | 8                             | 10                         | 10                          | 12                            | 12                         |

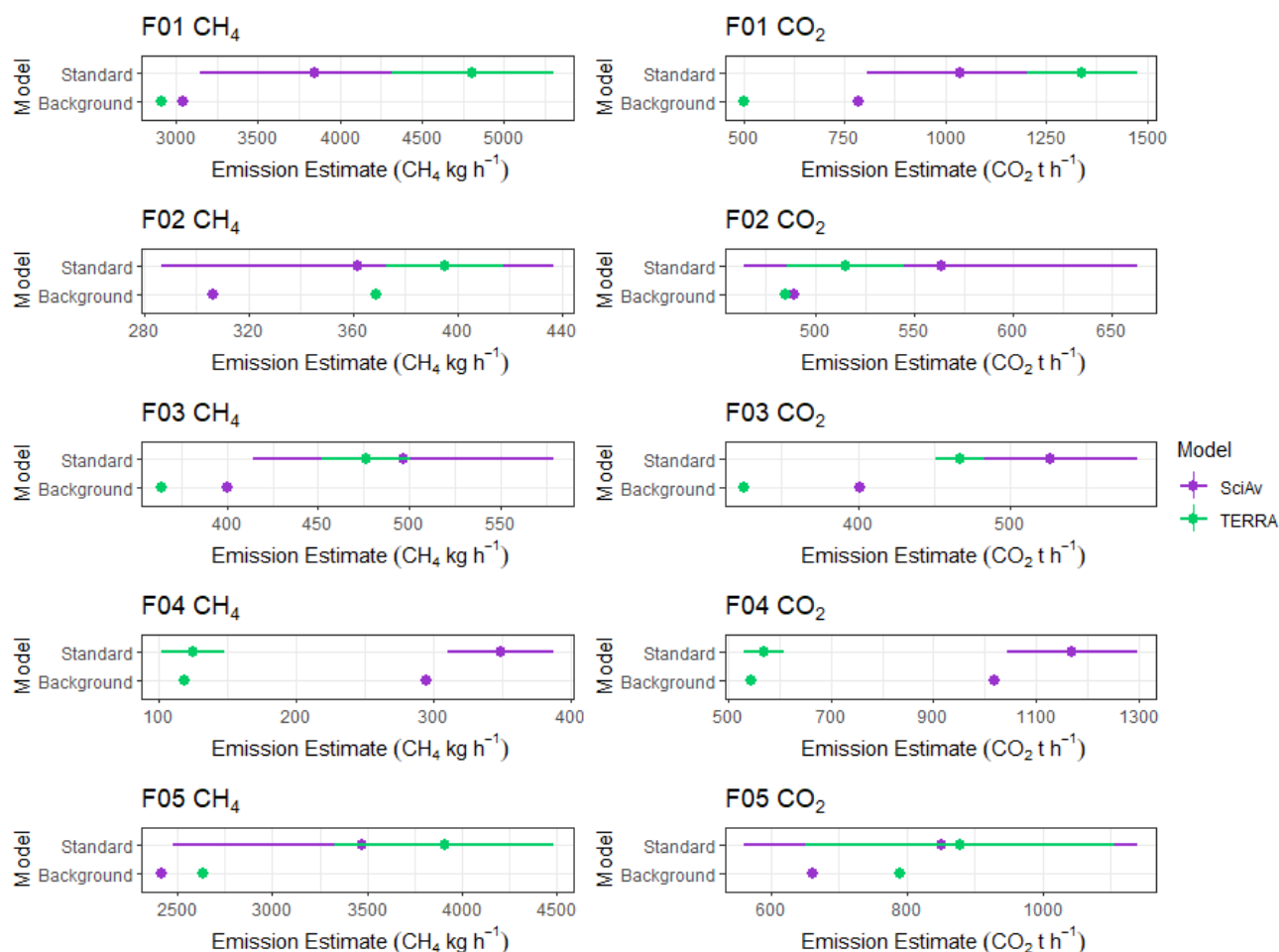


**Figure S 14: Algorithm estimates for CH<sub>4</sub> and CO<sub>2</sub> given the background mixing ratio fit of no emission plume extrapolation to the surface compared to the standard estimates.**

245 Table S 10 gives the percentage relative differences between each algorithm, and the standard deviation of the percentages for each surface extrapolation, calculated for the four surface extrapolations used for each method. In general, the choice in surface extrapolation varied less than the relative percentage difference between the algorithms. Fitting extrapolations with increasing emissions towards the surface increased agreement for F01 CO<sub>2</sub> from a percentage relative difference of 16% for the standard constant fit, to 7% using the linear fit.

250

255 **Table S 10: Percentage relative difference of estimates between algorithms, calculated as SciAv – TERRA, for each of the linear, Interpolate, constant and background surface extrapolations. The standard deviation between the percentages rounded to the nearest integer for each flight is given in the last column.**

|                         | Linear | Interpolate | Constant | Background | Standard<br>Deviation |
|-------------------------|--------|-------------|----------|------------|-----------------------|
| F01 CH <sub>4</sub> (%) | 9      | 5           | -12      | 5          | 9                     |
| F02 CH <sub>4</sub> (%) | -16    | -18         | -13      | -19        | 3                     |
| F03 CH <sub>4</sub> (%) | 6      | 8           | 8        | 9          | 1                     |
| F04 CH <sub>4</sub> (%) | 105    | 87          | 94       | 85         | 9                     |
| F05 CH <sub>4</sub> (%) | -5     | -4          | -2       | -9         | 3                     |
| F01 CO <sub>2</sub> (%) | -7     | 0           | -16      | 44         | 26                    |
| F02 CO <sub>2</sub> (%) | 2      | 1           | 5        | 1          | 2                     |
| F03 CO <sub>2</sub> (%) | 17     | 18          | 14       | 21         | 3                     |
| F04 CO <sub>2</sub> (%) | 62     | 59          | 66       | 61         | 3                     |
| F05 CO <sub>2</sub> (%) | -11    | -11         | -4       | -18        | 6                     |

260 To obtain a sense of the range of estimates from each algorithm a distribution of randomly sampled mean differences was created. For each flight and gas, a bootstrap analysis was applied by randomly sampling an estimate given one of the extrapolations for each method individually and the difference computed as:

$$difference = mean( Estimate_{SciAv} ) - mean( Estimate_{TERRA} ) \tag{6}$$

Analysis was run in Rstudio using the two.boot function from the simpleboot package (Peng, 2019). 5000 replications were  
 265 used for each bootstrap to obtain the distributional shape of the results. These distributions were used as a proxy for statistical confidence intervals (main text, Figure 8). They were used to estimate testing of the null hypothesis that estimates agree, and if the distributions do not overlap with zero then there is evidence that the algorithms differ.



270 1.7 Comparison Results and Significance Testing

The current SciAv method uses a binning method for integrating the profile points over altitude to estimate the overall emission estimate. This method can produce large flux divergence error terms when a small number of laps have been flown and divergence points differ greatly between laps, which can inaccurately estimate error if the variation is due to a trend such as emissions increasing to the surface. In these scenarios it may be beneficial to use trapezoidal integration rather than binning to estimate emissions. Rather than grouping into altitude bins the trapezoidal integration estimates the area under the curve by a trapezoidal fit between each point. Trapezoidal integration fits the area by altitude between a divergence of zero and the positive divergence calculated for each lap using the lines connecting the points. This method parallels the calculation of the SciAv divergence error term whilst avoiding the potential bias from a small number of flight laps.

280 Table S 11 gives the SciAv trapezoidal integration method estimates. Figures S 15 A – 15 E show the SciAv profiles given the trapezoidal integration method. Surface extrapolations are fit from the lowest mean divergence lap estimate. The estimated end point for the surface extrapolation does not change between the two integration methods as it is determined by fitting curves by the position of the points and fitting height. As the surface extrapolation points were the same for both profiles which caused the F01 trapezoidal profiles to decrease despite their noticeable increasing to surface trend (Figure S 15 A). A less conservative fitting height procedure would likely produce a large range in emission estimates, and should be explored if the trapezoidal method is adapted, as it could produce an extrapolation truer to the nature of the divergence profile.

285

**Table S 11: SciAv emission rate estimates using trapezoid integration.**

| Flight | Surface Extrapolation | CH <sub>4</sub> Emission (kg h <sup>-1</sup> ) | CO <sub>2</sub> Emission (t h <sup>-1</sup> ) |
|--------|-----------------------|--|---|
| F01    | Constant              | 4840   | 1350  |
| F01    | Background            | 3130   | 831   |
| F01    | Linear                | 4600   | 1300  |
| F01    | Interpolate           | 3980   | 1090  |
| F01    | Linear Weighted       | 4770   | 1350  |
| F01    | Averaged              | 4730   | 1330  |
| F02    | Constant              | 352  | 550   |
| F02    | Background            | 302  | 483   |
| F02    | Linear                | 355  | 550   |
| F02    | Interpolate           | 327  | 517   |
| F02    | Linear Weighted       | 354  | 557   |

|     |                 |      |      |
|-----|-----------------|------|------|
| F02 | Averaged        | 354  | 552  |
| F03 | Constant        | 530  | 530  |
| F03 | Background      | 426  | 375  |
| F03 | Linear          | 532  | 527  |
| F03 | Interpolate     | 478  | 453  |
| F03 | Linear Weighted | 530  | 545  |
| F03 | Averaged        | 531  | 534  |
| F04 | Constant        | 338  | 1120 |
| F04 | Background      | 301  | 1060 |
| F04 | Linear          | 339  | 1130 |
| F04 | Interpolate     | 320  | 1090 |
| F04 | Linear Weighted | 339  | 1150 |
| F04 | Averaged        | 339  | 1130 |
| F05 | Constant        | 3780 | 797  |
| F05 | Background      | 2540 | 619  |
| F05 | Linear          | 3830 | 740  |
| F05 | Interpolate     | 3160 | 708  |
| F05 | Linear Weighted | 3800 | 739  |
| F05 | Averaged        | 3800 | 759  |

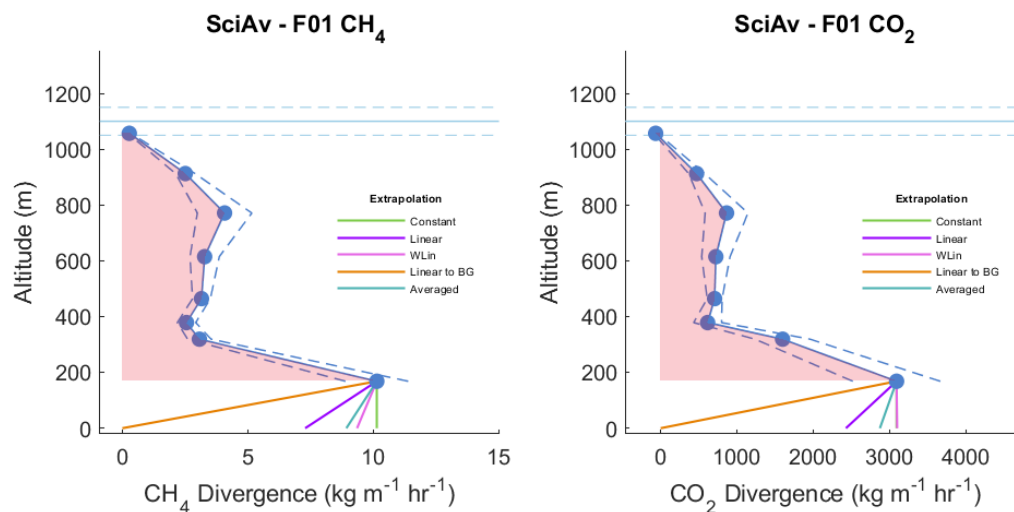


**Figure S 15 A.**

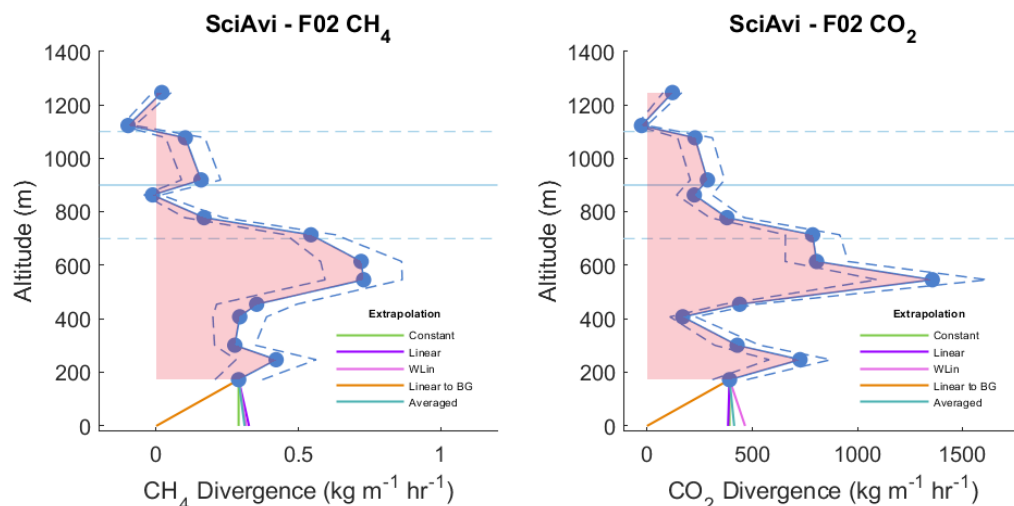


**Figure S 15 B.**

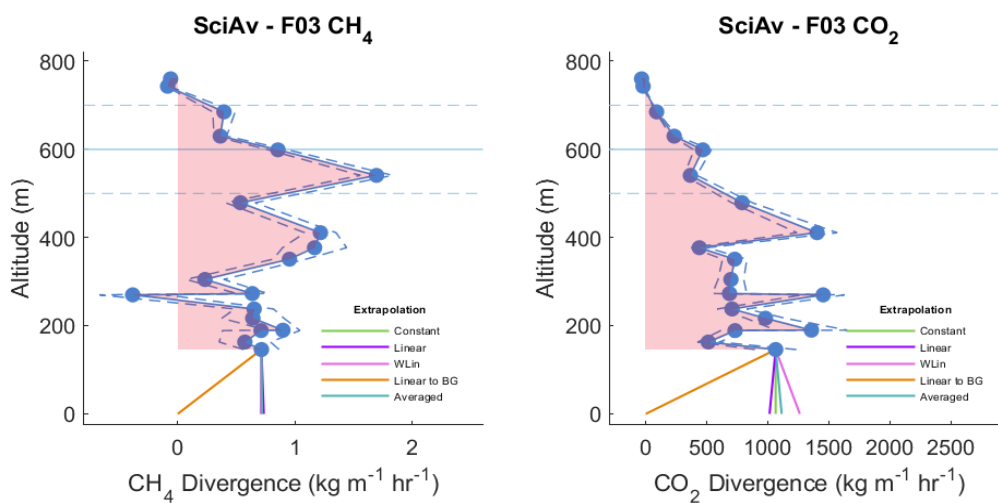


**Figure S 15 C.**

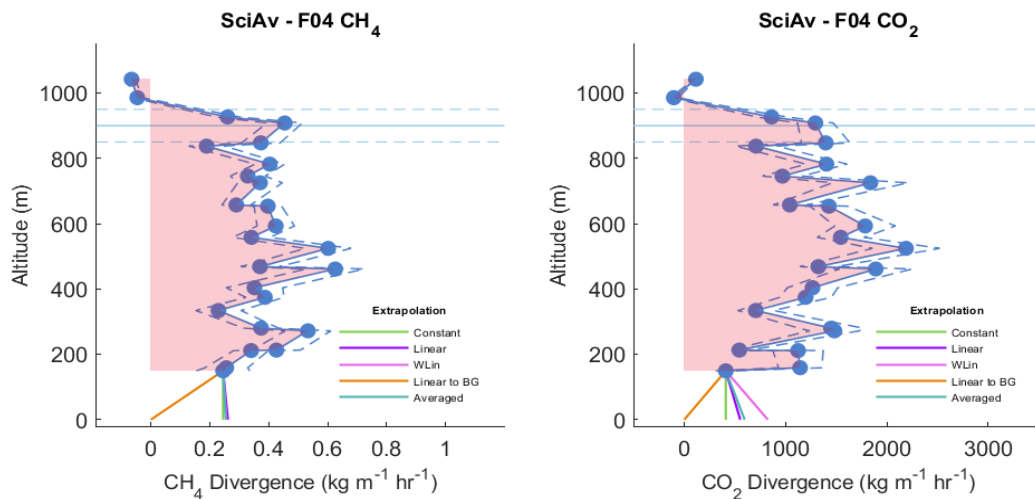


Figure S 15 D.

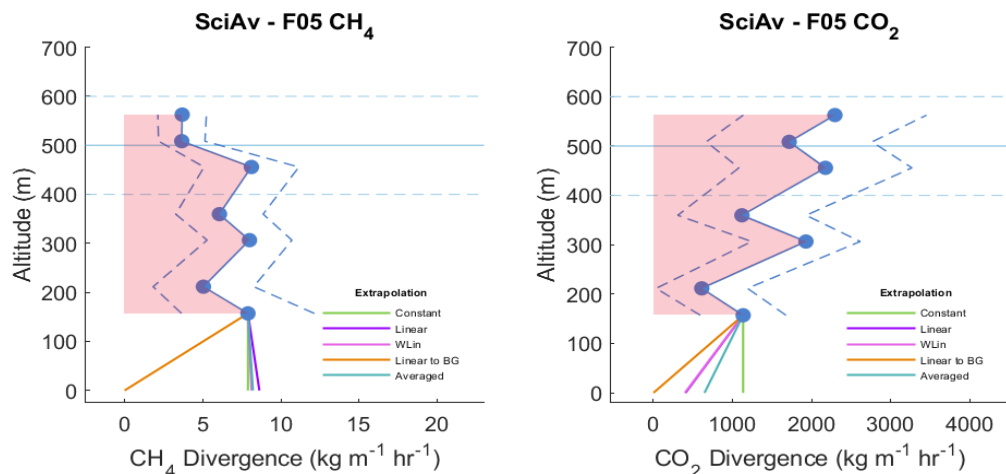
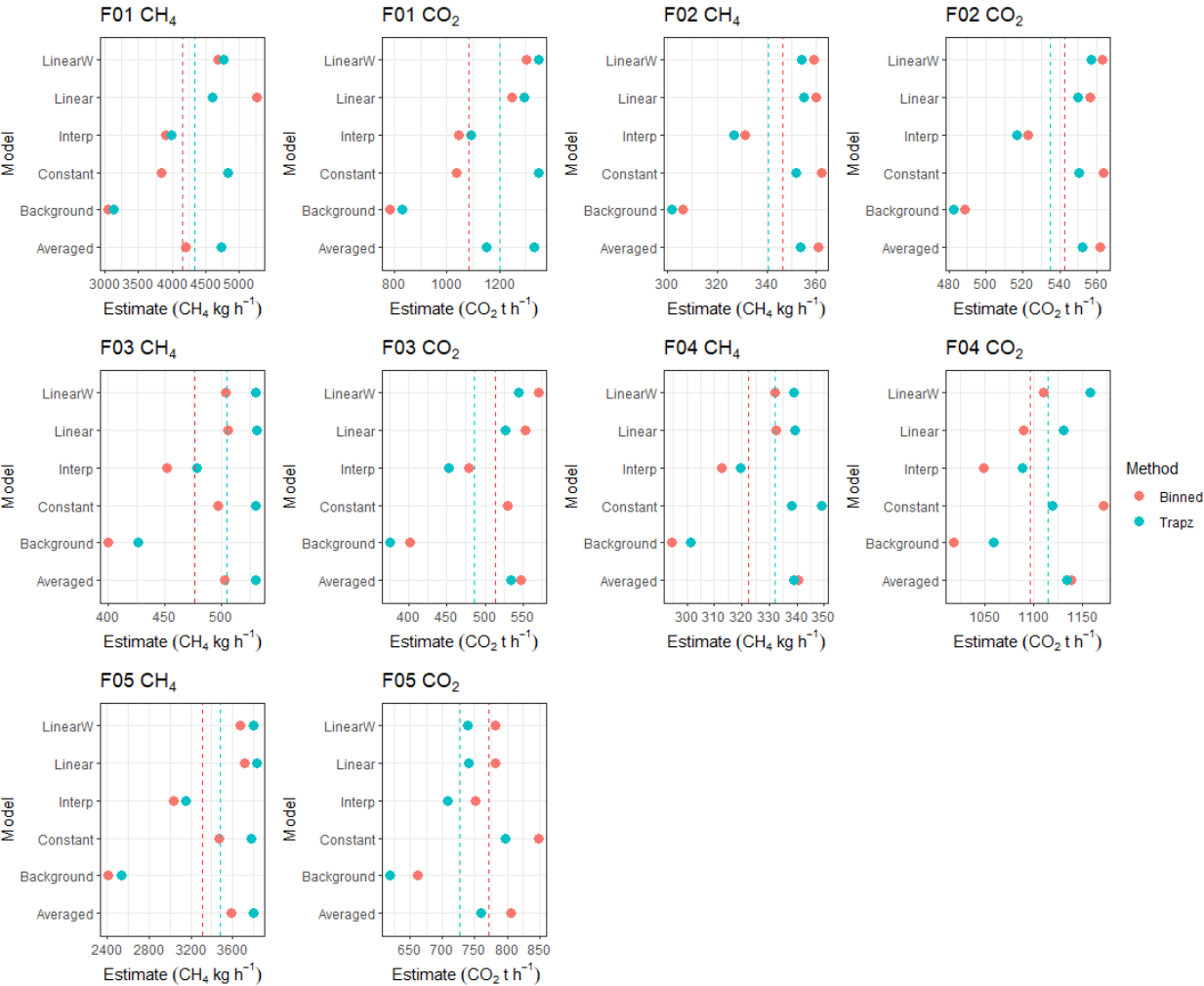


Figure S 15 E.

Figure S 5: A - E of the SciAv profiles for flights F01 through F05. The blue points are the estimated flux divergence for each lap which are connected to show profile shape with the associated error (a dashed blue line). The red area is the trapezoidal integrated area of the blue divergence points excluding the surface extrapolation. The boundary layer height is drawn in light blue with error bars (light blue dashed lines). The five surface extrapolations are drawn from the bottom of the lowest blue divergence point.

Figure S 16 show the binned estimates compared to the trapezoidal (Trapz). No systematic pattern is evident that would indicate that one integration method produces consistently larger or smaller emissions estimates. There is a systematic gap between estimates that could be attributed to the use of different extrapolation points. The binned method uses the lowest bin for extrapolation, whereas the trapezoidal method uses the lowest divergence point.



**Figure S 6: SciAv emission estimates of CH<sub>4</sub> (kg h<sup>-1</sup>) and CO<sub>2</sub> (t h<sup>-1</sup>) derived using both a binning (red) and trapezoidal (blue) integration method. Mean values for each method are shown as a dotted line.**

Inspecting Figure S 16 there is a larger variation between estimates due to the chosen surface extrapolation than integration method. There was one exception, there is a larger difference between the integration types when a constant extrapolation is chosen for F01. This flight has an increasing to surface profile point, and because the lowest divergence point differs greatly from the location of the lowest bin estimate, the extrapolation fits differ. Applying an appropriate surface extrapolation that follows the shape of the profile remedied the difference between integration methods.

Percentage relative standard deviations (%RSD) were calculated (Table S 12) to estimate the deviation in the surface extrapolation estimates given the binning and trapezoidal approaches to integrating the SciAv lap divergence data. These were compared to the %RSD of the difference between the two integration methods. Table S 13 gives the standard deviations of the surface extrapolation estimates for each integration method and the standard deviation for the difference between integration methods for all five flights. Table S 14 gives the results from significance tests on the differences between the estimates. The choice of surface extrapolation leads to a greater standard deviation than the choice of integration method. Results showed that the range in emission output was a factor of ~ 3 times larger for the range in surface extrapolation estimates than the difference between using a binned or trapezoidal integration. The choice in the surface extrapolation affected the range of emission outputs more than the integration type.

**Table S 12: Percentage relative standard deviations (RSD) calculated from the set of seven SciAv surface extrapolations given a binned or trapezoidal integration method and for the difference between the two. The mean of each %RSD is calculated amongst all flights.**

|                     | F01<br>CH <sub>4</sub> | F02<br>CH <sub>4</sub> | F03<br>CH <sub>4</sub> | F04<br>CH <sub>4</sub> | F05<br>CH <sub>4</sub> | F01<br>CO <sub>2</sub> | F02<br>CO <sub>2</sub> | F03<br>CO <sub>2</sub> | F04<br>CO <sub>2</sub> | F05<br>CO <sub>2</sub> | Mean |
|---------------------|------------------------|------------------------|------------------------|------------------------|------------------------|------------------------|------------------------|------------------------|------------------------|------------------------|------|
| Binned<br>%RSD      | 18                     | 7                      | 9                      | 6                      | 15                     | 17                     | 6                      | 12                     | 5                      | 8                      | 10   |
| Trapezoid<br>% RSD  | 15                     | 7                      | 9                      | 5                      | 15                     | 17                     | 5                      | 14                     | 3                      | 8                      | 10   |
| Difference<br>% RSD | 12                     | 1                      | 1                      | 2                      | 2                      | 9                      | 1                      | 3                      | 3                      | 0                      | 3    |

**Table S 13: Standard deviation of the surface extrapolation estimates for each integration and the difference between integration method extrapolation estimates (calculated as: binned estimate – trapezoidal estimate).**

|  | SD Binned<br>Extrapolation Estimates | SD Trapezoidal<br>Extrapolation Estimates | SD Difference in Methods<br>Extrapolation Estimates |
|--|--------------------------------------|---|---|
| CH <sub>4</sub> (kg hr <sup>-1</sup> ) | 1740                                 | 1810                                      | 581   |
| CO <sub>2</sub> (t hr <sup>-1</sup> )  | 274                                  | 315                                       | 139   |

**Table S 14: Results of parametric (weighted t-test) and non-parametric (Wilcoxon signed-rank test) significance testing of differences between the two SciAv integration method, by calculating the mean of the estimates for each flight and tested over the whole set of five flights.**

|                 | Weighted t-test: p-value | Weighted t-test: t-value | Wilcoxon signed-rank<br>test: p-value | Wilcoxon signed-rank<br>test: V |
|-----------------|--------------------------|--------------------------|---------------------------------------|---------------------------------|
| CH <sub>4</sub> | 0.952                    | -0.062                   | 0.188                                 | 2                               |
| CO <sub>2</sub> | 0.952                    | -0.062                   | 1                                     | 8                               |

To further compare the two methods of integrated a distribution of the mean differences for each flight was computed by bootstrapping the mean difference between randomly sampled estimates. The mean difference was computed as:

$$difference = mean(SciAvEstimate_{Binned}) - mean(SciAvEstimate_{Trapez}) \tag{7}$$

As shown in Figure S 17, the distributions for all flight samples of each emission type cover zero indicating that the two integration methods produce similar estimates. The trapezoidal integration may be a useful method for profiles with a small number of laps, but the choice of an appropriate surface extrapolation has a larger effect on the emission estimate than the type of integration used. The SciAv divergence error term could be calculated by using the lap data and bootstrapping the trapezoidal integration over thousands of profile points that are randomly sampled within the uncertainty of each point to estimate the random sampling error between each lap by altitude. A surface extrapolation term could be derived following methods used in TERRA by assessing the maximum percent change between plausible extrapolations.

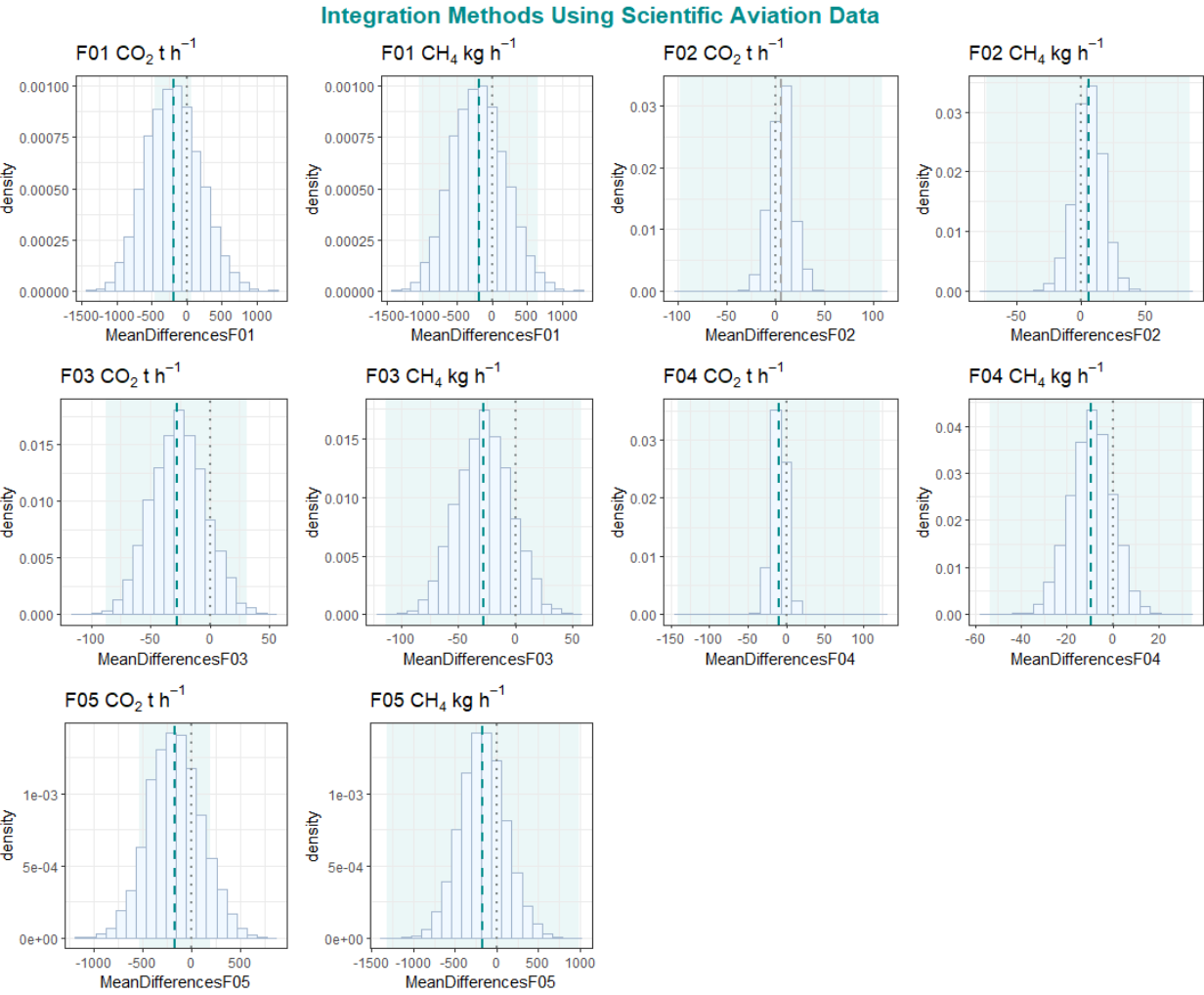


**Figure S 17: Distributions of the mean difference between all SciAv fits of CH<sub>4</sub> and CO<sub>2</sub>, given the binning compared to the trapezoidal integration methods, in light blue. The mean difference between the standard estimates is plotted as a teal dashed line and the range in the estimate as the light teal box behind the distribution. A grey dot dashed line is drawn at zero as a reference point for the location of exact agreement between the methods.**

## Box-flight Algorithm Assumptions Investigated

### 1.8 Flight Screening and Analysis of Meteorological Conditions During Flight F04

The potential cause of the non-stationarity of F04 was thoroughly investigated. Analysis of the raw data and emission profiles indicates that the emission plume itself was non-stationary as the mixing ratios enhancements noticeably differed between the upwards and downwards portion of the flight, but other potential causes such as changing meteorological conditions were inspected. Along with the flight screening provided by Scientific Aviation and Alberta Airshed Stewardship, conditions were assessed using the full data and then split into upwards (ascending) and downwards (descending) sections for comparison. The various analysis provided in this document supports the conclusion that meteorological conditions were not the cause of the F04 non-stationarity.

Prior to this study, Scientific Aviation and Alberta Airshed Stewardship performed a screening of all flights in the AEP-NOAA-Scientific Aviation 2017-2018 Alberta Oil Sands Flight Campaign. This process includes looking at 'circle' files and assessing the wind direction and mixing ratio measurement for each lap. The circle files help detect plume capture, non-stationarity of the wind, and any upwind flux that is not coming from the intended emission source. The SciAv lap divergence profiles are also inspected for plume capture and the shape of the plume. Stationarity and consistency of the wind data was deemed good, the plume was assessed as fully captured, and there was negligible upwind flux entering the box.

The non-stationarity of F04 was not confirmed until post-hoc analysis was applied by Environment and Climate Change Canada. The TERRA step of kriging the data uses the lap data to produce spatially gridded emission mixing ratios. Figure S 20 shows the middle step of gridded screen for F04 CH<sub>4</sub>. Some boxes contained a high (red) emission and a low (blue) emission enhancement (Figure S 18) which is evidence of non-stationarity as the plume and background mixing ratios changed over time. The change in mixing ratios may have occurred due to changing operating conditions at or near the facility, but operations conditions were not shared by the facility. The non-stationarity of the emission plume biased the TERRA estimates as the large mixing ratio differences in each square led to lower estimates from the kriging. For TERRA, there is a noticeable difference in the CH<sub>4</sub> mixing ratios in the upward flight compared to the downward, with higher mixing ratios (red) detected in the ascending portion of the flight (Figure S 19).



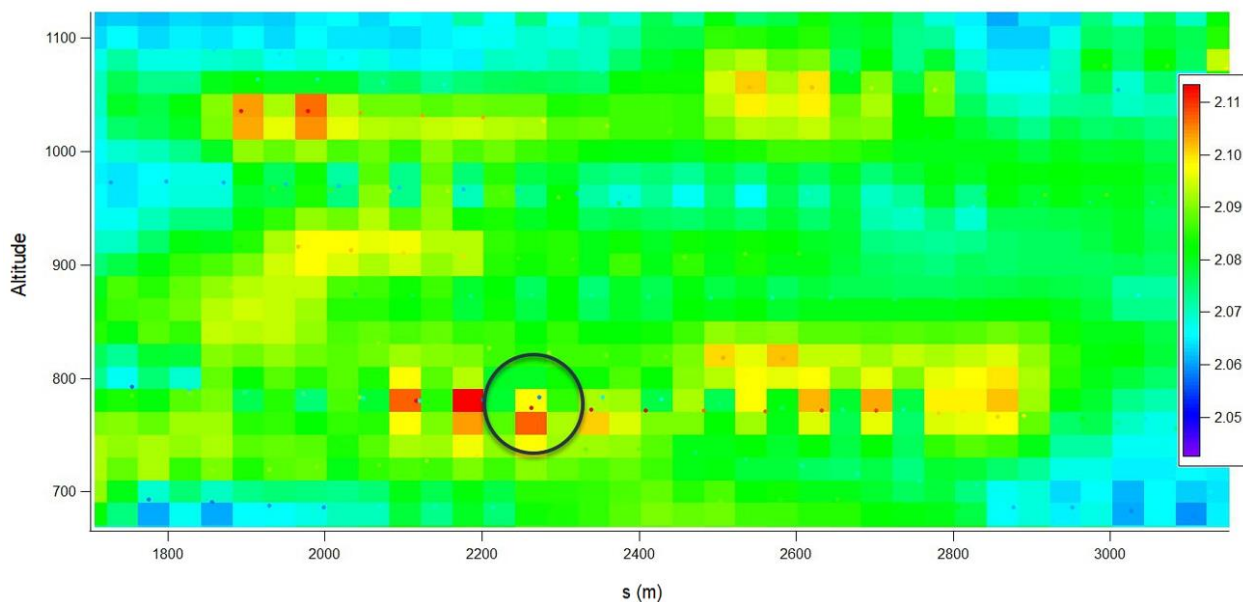


Figure S 18: A zoomed in look at the final F04 CH<sub>4</sub> box of kriging-interpolated data. A black circle is drawn around a gridded square that contained a large red enhancement at the same location as a low blue mixing ratio. The square was averaged to a yellow CH<sub>4</sub> value. Imagery provided by Environment and Climate Change Canada.

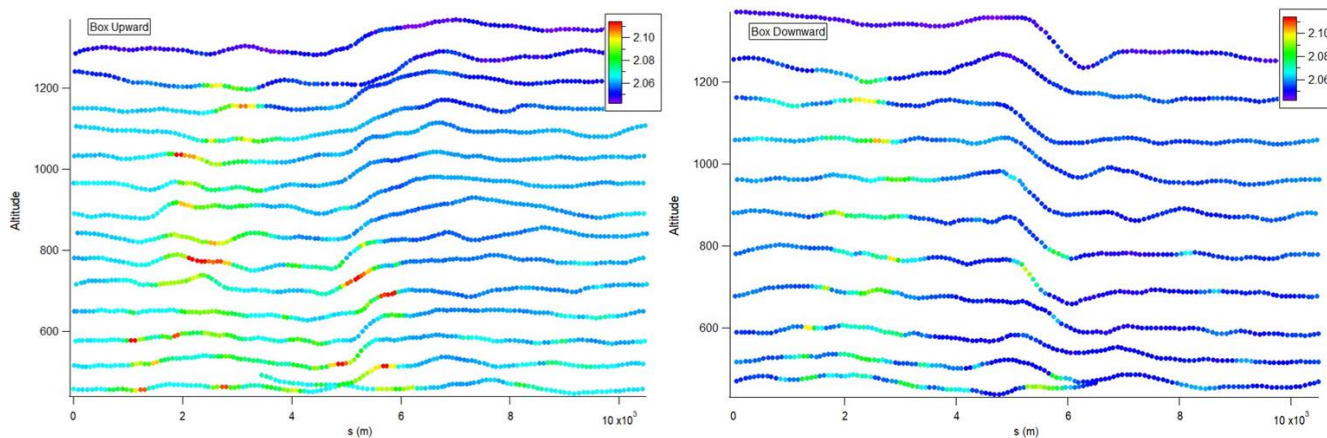


Figure S 19: Per lap CH<sub>4</sub> mixing ratio screen data for the box upward (left) and downward (right) prior to kriging of the data. Imagery provided by Environment and Climate Change Canada.

As part of the meteorological conditions' analysis, the stability of the boundary layer was assessed. To thoroughly investigate conditions multiple variables were calculated to produce multiple estimates of the boundary layer. Following previous calculations for estimating the boundary layer from aircraft flight data (Dai et al., 2014) variables were computed: gradient  
385 Richardson number, bulk Richardson number, change in virtual temperature, change in potential temperature, and the change in virtual potential temperature. The boundary layer height was estimated from the maximum of each of these variables to assess any changes during the flight up versus down. These values were also compared to the SciAv estimate that was provided which was estimated the day of the flight. The calculated maximum values used to estimate the boundary layer are plotted in Figure S 20 for the full, upwards, and downwards F04 flight segments. Analysis by Dai et al. 2014 suggest the best practice is  
390 to estimate the boundary layer at maximum change in the virtual potential temperature ( $\max VPT/dz$ ). For this flight, the boundary layer estimate is near SciAv's estimate and appears stable. If the meteorological conditions caused a significant shift in the boundary layer this would likely show up during the reanalysis. The consistency in boundary layer estimates for the flight up versus down further indicates that the boundary layer was stationary during the flight.

395 Thorough analysis of the boundary layer, and the wind components supports the conclusion that meteorological conditions were not the source of the non-stationarity of the emission plume for F04. Ruling out changing meteorological conditions leaves a change in the background mixing ratio, or a change in the facility emissions during the flight as potential causes of the non-stationarity. However, the cause of the non-stationarity of the emission plumes for F04 remains unknown as there was no independent measurement of the background mixing ratio during sampling, and the operating conditions near and at the  
400 facility were not shared.

Boundary Layer Estimates F04 : 2017-08-14

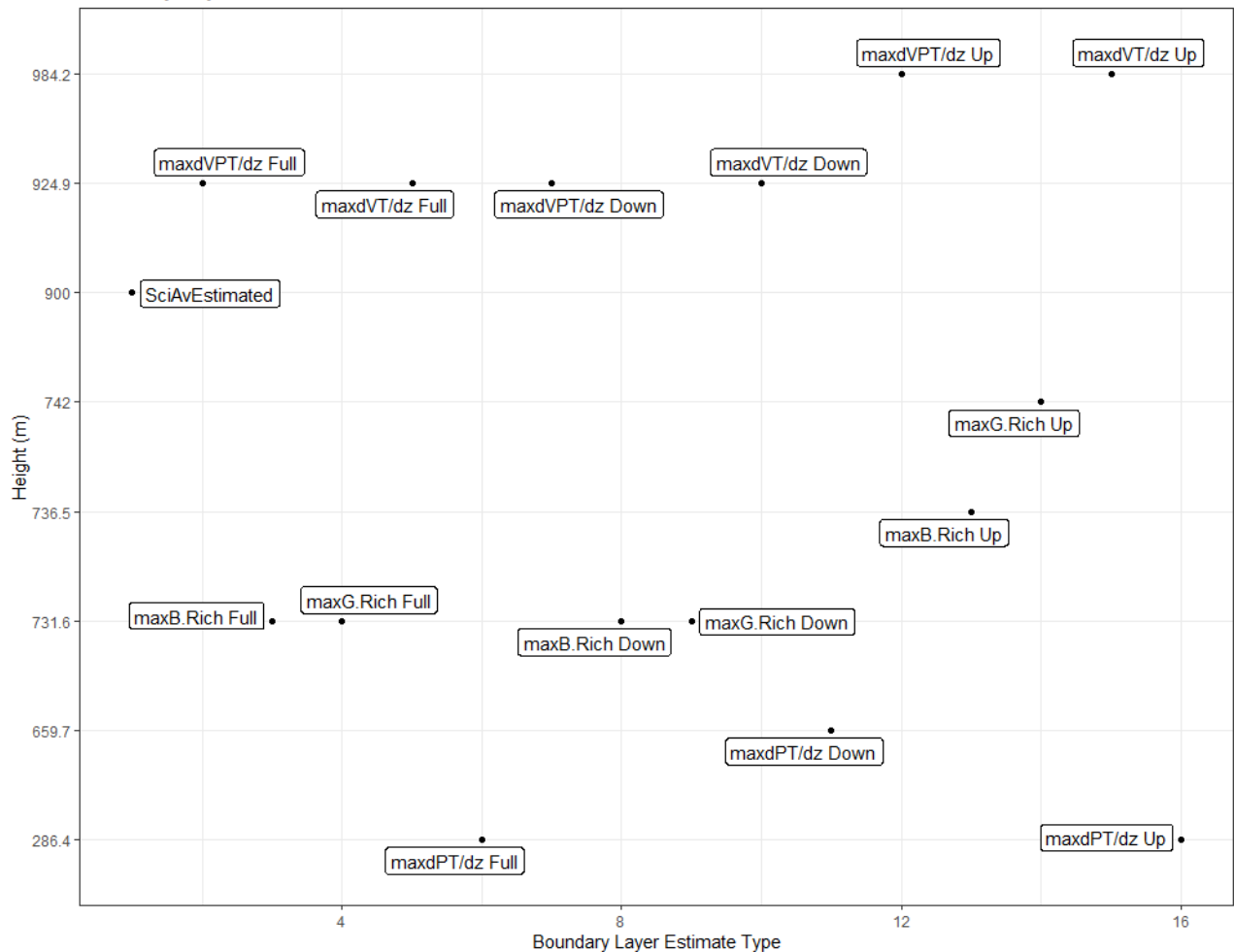


Figure S 20: The five boundary layer estimates for the full, up and down F04 flight segments plotted as the maximum: gradient Richardson number (maxG.Rich), bulk Richardson number (maxB.Rich), change in virtual temperature (dVT/dz), change in potential temperature (dPT/dz), and change in virtual potential temperature (dVPT/dz). The acronym dz is the change in altitude above ground level. The y-axis gives the estimated boundary layer in meters above ground level.

## References

- Conley, S., Faloona, I., Mehrotra, S., Suard, M., Lenschow, D. H., Sweeney, C., Herndon, S., Schwietzke, S., Pétron, G., Pifer, J., Kort, E. A., and Schnell, R.: Application of Gauss's theorem to quantify localized surface emissions from airborne measurements of wind and trace gases, *Atmos. Meas. Tech.*, 10, 3345–3358, <https://doi.org/10.5194/amt-10-3345-2017>, 2017.
- Dai, C., Wang, Q., Kalogiros, J. A., Lenschow, D. H., Gao, Z., and Zhou, M.: Determining Boundary-Layer Height from Aircraft Measurements, *Boundary-Layer Meteorol.*, 152, 277–302, <https://doi.org/10.1007/s10546-014-9929-z>, 2014.
- Gordon, M., Li, S. M., Staebler, R., Darlington, A., Hayden, K., O'Brien, J., and Wolde, M.: Determining air pollutant emission rates based on mass balance using airborne measurement data over the Alberta oil sands operations, *Atmos. Meas. Tech.*, 8, 3745–3765, <https://doi.org/10.5194/amt-8-3745-2015>, 2015.
- Peng, R. D.: simpleboot: Simple Bootstrap Routines, [code], <https://github.com/rdpeng/simpleboot>, 2019.